indicate that the iNOS expression was selectively inhibited by iNOS antisense DNA plasmid and was efficiently reduced to the same level as without cytokine stimulation.

NADPH diaphorase staining. NADPH diaphorase staining is an index of NOS activity (6). NADPH diaphorase was distinctly recognized in a wild-type cell line, a vector control line, and a sense line after the stimulation of TNF-α and IL-1β (Fig. 3). In contrast, NADPH diaphorase was less detected in the antisense lines.

Effects of cytokines on NO production. Unstimulated MC3T3-E1 cells released a basal amount of NO detected as nitrate/nitrite (2.47 ± 0.48 ~ 3.17 ± 0.32 μM) in all cell lines (Fig. 4). After cytokine stimulation for 24 h, the wild-type cell line and the vector control line showed a significantly high level of nitrate/nitrite accumulation (48.1 ± 1.5 and 41.4 ± 2.2 μM, respectively). The sense plasmid-induced cell line also produced a high level of nitrate/nitrite accumulation. The mean of three sense lines was 44.5 ± 6.7 μM. On the other hand, the antisense lines produced only 22–34% NO compared with that of the sense lines in response to the cytokines (mean of 3 antisense lines was 12.1 ± 0.92 μM). These results indicate that the production of NO after cytokine stimulation was significantly suppressed in the antisense lines ($P < 0.01$).

Effects of iNOS antisense on proliferation in the presence of cytokines. An MTS assay was used to analyze the effects of iNOS antisense on the proliferation of cells treated with cytokines. As shown in Fig. 5, antisense cell lines significantly promoted the growth even if they were treated with cytokines. Therefore, it is indicated that iNOS antisense partially attenuated the reduction of proliferation in the presence of cytokines.

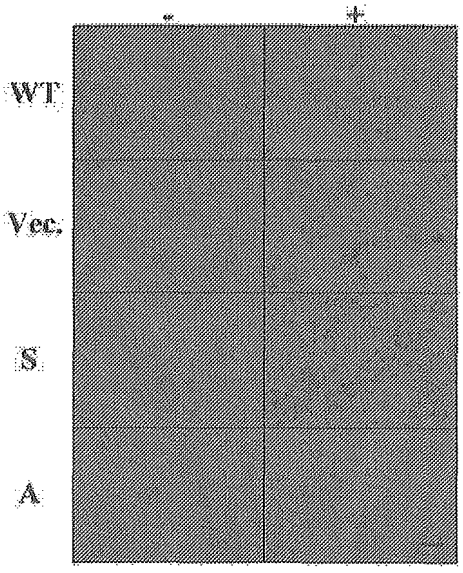

Fig. 3. NADPH diaphorase activity after cytokine stimulation. NADPH diaphorase activity after cytokine stimulation for 24 h found in wild-type cells was reduced in antisense. WT, wild-type cells; Vec, empty vector control line; S, sense lines; A, antisense lines; −, unstimulated; +, cytokine stimulated. Bar length, 100 μm.

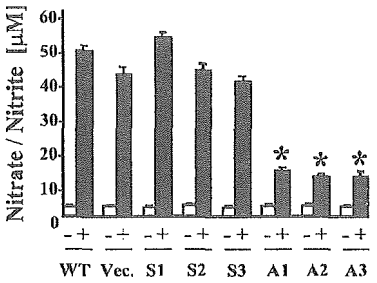

Fig. 4. Effects of cytokines on nitric oxide (NO) production in MC3T3-E1 cells. After cytokine stimulation for 24 h, NO is detected as nitrate/nitrite as described in MATERIALS AND METHODS. Open bars, NO production in unstimulated cells (−); filled bars, NO production in stimulated cells (+). Results are means ± SD; $n = 12$ experiments. *$P < 0.01$ relative to *antisense lines A1–A3*.

ALPase activity in transformed MC3T3-E1 cells. Stimulation by TNF-α and IL-1β reduced the ALPase activity in the wild-type, vector control, and sense-transduced lines compared with that in unstimulated cells (Fig. 6). The mean reduction in ALPase activity by cytokines in the sense lines was 59.2 ± 17% that of the unstimulated control ($P < 0.01$). In contrast, the ALPase activity of the antisense lines did not change significantly (mean of 3 cell lines was 111.5 ± 17%), indicating that the antisense lines did not influence the ALPase activity secondary to the cytokine stimulation.

Expression of marker genes on osteoblastic differentiation. To investigate the effects of iNOS antisense on the expression of the differentiation markers in osteoblasts, we performed semiquantitative RT-PCR using specific primers for COL I, ALPase, OSC, and Cbfa1. OSC mRNA was constitutively expressed in unstimulated cells (Fig. 7*A*, *top*). However, after cytokine stimulation for 48 h, the gene expression was reduced in the wild-type, vector control, and sense lines. The antisense cell lines meanwhile showed higher levels of gene expression compared with the sense lines. The relative gene expression levels after cytokine stimulation were

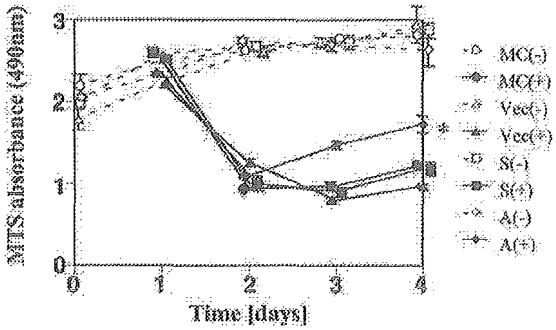

Fig. 5. Cell proliferation assay. Each cell line was incubated at a density of 4 × 10 cells/well in 96-well plates for 24 h and then cultured in the absence or presence of cytokines and cultured for 3 more days. For determination of cell proliferation, 3-(4,5-dimethylthiazol-2-yl)-5-(3-carboxymethoxyphenyl)-2-(4-sulfophenyl)-2H-tetrazolium (MTS), inner salt assay was performed on *days 0, 1, 2, 3,* and *4*. Broken and solid lines represent absorbance of unstimulated (−) and stimulated (+) cells, respectively. Results shown are means ± SD; $n = 10$. *$P < 0.01$ relative to stimulated control.

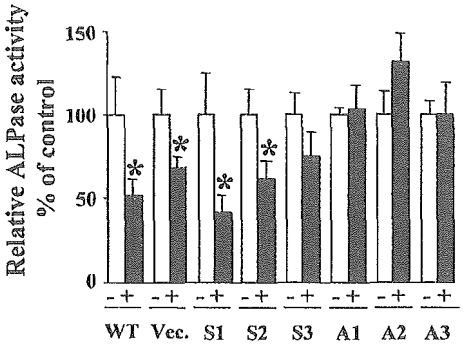

Fig. 6. Effects of cytokines on alkaline phosphatase (ALPase) activity. After cytokine stimulation for 48 h, relative ALPase activity was compared with unstimulated cells (−). Open bars, ALPase activity in unstimulated cells; filled bars, ALPase activity in stimulated cells. Results are means ± SD; $n = 12$. *$P < 0.01$ relative to unstimulated control.

compared with the unstimulated control level (Fig. 7*A*, *bottom*). The sense lines decreased to 52 ± 9% (mean of 3 cell lines) compared with the unstimulated control ($P < 0.01$), whereas the antisense increased to 227 ± 92% (means of 3 cell lines, $P < 0.01$). After the normalization with GAPDH, the sense line decreased to 44 ± 8% (mean of 3 cell lines) compared with the unstimulated control ($P < 0.01$), and the antisense increased to 284 ± 149% (mean of 3 cell lines, $P < 0.01$). Similarly, we assessed the expression of COL I, ALPase, and Cbfa1 using representative cell lines (S2 and A2; Fig. 7*B*). These results indicate that the antisense cell line prevented the reduction of the relative mRNA levels of ALPase and Cbfa1 after cytokine stimulation compared with the other controls. Although cytokines showed a variable tendency to inhibit COL I mRNA in the three control cell lines, all of the antisense cell lines prevented the inhibition of COL I mRNA with cytokines.

Immunodetection of $ONOO^-$ by anti-NT antibody. The NT residue on protein is a stable product of $ONOO^-$ reaction (9). The wild type (Fig. 8*C*), the vector control line (Fig. 8*E*), and the sense line (Fig. 8*G*) showed an intense NT expression after cytokine stimulation, whereas the antisense line (Fig. 8*I*) did not exhibit elevated levels of NT expression (Fig. 8). These

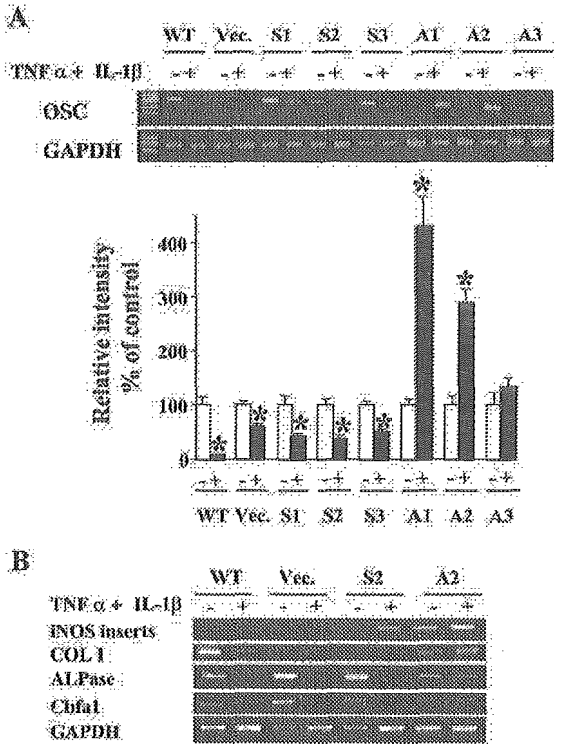

Fig. 7. Expression of marker genes on osteoblastic differentiation. PCR conditions were determined such that the band intensity had a linear relationship with an increase in the cycle number [30 cycles for type I collagen (COL I), 26 cycles for ALPase, osteocalcin (OSC), and core binding factor (Cbfa1)]. *A*: iNOS inserts (see Fig. 1). *B*: COL I, ALPase, Cbfa1, and GAPDH. Expected product sizes for COL I, ALPase, OSC, Cbfa1, and GAPDH are 656, 373, 276, 373, and 988 bp, respectively. Results of OSC quantified by densitometry are shown in *A*, *bottom*. mRNA levels of OSC are compared with unstimulated control after normalization with GAPDH and quantification by image analysis. Values are means ± SD of combined results from 3 separate experiments. *$P < 0.01$ relative to unstimulated control.

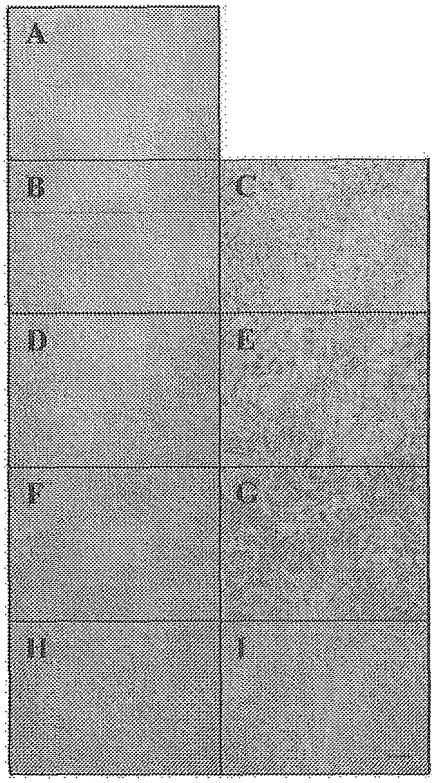

Fig. 8. Immunocytochemistry of nitrotyrosine (NT) after cytokine stimulation. After cytokine stimulation for 48 h, immunocytochemistry of NT was performed. NT residues are stable markers of $ONOO^-$ synthesis. *A*: negative control in wild-type MC3T3-E1 cells; *B*: unstimulated wild-type cells; *C*: positive control in wild-type cells after cytokine stimulation; *D*: unstimulated empty vector control line; *E*: empty vector control line after cytokine stimulation; *F*: unstimulated sense line; *G*: sense line after cytokine stimulation; *H*: unstimulated antisense line; *I*: antisense line after cytokine stimulation. Note that the antisense line after cytokine stimulation decreased the immunoproduct of NT. Bar length, 100 μm.

results were quantified by densitometry. The levels of staining intensity were 15 ± 2, 17± 7, 20 ± 8, and 21 ± 5 in the wild-type, vector control, sense, and antisense lines, respectively (Fig. 8, *B*, *D*, *F*, and *H*). After cytokine stimulation, the corresponding levels of staining intensity were 88 ± 20, 75 ± 7, 84 ± 4, and 33 ± 10 (Fig. 8, *C*, *E*, *G*, *I*). These results suggest that MC3T3-E1 antisense cell lines, which inhibit the expression of iNOS after cytokine stimulation, decreased the production of NO and $ONOO^-$ ($P < 0.01$).

DISCUSSION

The purpose of our investigation is to examine whether the specific inhibition of iNOS by antisense DNA plasmid would prevent the proinflammatory cytokine-induced reduction in osteoblastic differentiation. One essential drawback to using chemical inhibitors is its apparent inability to discriminate between the different isoforms of NOS and its additional functions (5). Moreover, although antisense oligonucleotides are generally used as antisense techniques to hybridize to specific RNA sequences, the antisense oligonucleotides may not always demonstrate a significant effect on the target mRNA for long-lasting analysis (17, 23, 28, 38) and must be added repeatedly to the culture medium at high concentrations. Furthermore, there are no decisive systems to deliver them efficiently to the target site through the cell membrane (17, 28). In addition, it has been found that antisense oligonucleotides have many effects other than the gene action, such that they may adsorb intracellular proteins and activate the immune systems (25, 42). For these reasons, the use of antisense plasmid was chosen for the direct blockade of the iNOS pathway, without impinging on constitutive NOS-dependent events, and to make it possible to select transformed cell lines for long-term analysis.

Previously, several groups have reported that, in murine macrophages and endothelial cells, iNOS is inhibited by plasmid DNA that directed the production of iNOS antisense RNA (7, 8, 37). However, we report on anti-inflammatory effects in osteoblastic cells with this iNOS antisense technique for the first time. We designed the 213-bp fragment of the iNOS region so that it covered the ATG initiation codon of the murine iNOS gene. Although further experiments are required to create increasingly efficient constructs, this antisense construct, including the noncoding region, demonstrated effective inhibition of iNOS gene expression and suppression of the biological function of NO.

Proinflammatory cytokines, such as TNF-α and IL-1β, are well known to be the most potent stimulators of bone resorption (4, 27) and to induce high levels of NO production in bone (10, 24, 34, 40). Interestingly, several groups have shown that these high concentrations of NO inhibit osteoclast formation and activity, which elevate with cytokine stimulation (6, 30, 32, 36). In contrast, two- to threefold inhibition of OSC synthesis (14, 20, 21, 39) and the reduction of ALPase activity with a combination of the two cytokines, TNF-α and IL-1β, have been confirmed in previous studies in osteoblasts (20, 21). Based on our experience with NO donor, it was also revealed that NO directly facilitated the levels of ALPase activity in osteoblastic cells (20). Despite the differentiation-enhancing effect of an NO donor, NO, especially derived from iNOS, appears to potentiate the inhibitory effects with a treatment of the two cytokines, TNF-α and IL-1β, on osteoblast activity in vitro.

Recent studies in iNOS knockout (KO) mice by van't Hof et al. (40) have shown that activation of the iNOS pathway is essential for IL-1-stimulated bone resorption, both in vitro and in vivo. Their coculture studies indicate that osteoblasts are the main source of NO and that osteoblast-derived NO acts in a paracrine and autocrine fashion on the bone component to promote IL-1-induced bone resorption. Furthermore, Armour et al. (3) have shown that apoptosis of osteoblasts and osteocytes contributes to inflammation-induced bone loss and suggested that the deleterious effects of iNOS activation and inflammation on bone may be relatively specific for mature osteoblasts. These findings strongly suggest that iNOS activation in osteoblasts may contribute to inflammatory diseases, inducing bone loss by suppressing bone formation (2, 15, 18). Another study in eNOS KO mice has shown that osteoblasts derived from eNOS KO mice reduce rates of growth when compared with the wild type and are less well differentiated, as reflected by lower levels of ALPase (1). These data suggest that eNOS is essential for normal osteoblast differentiation and function. These data support our hypothesis that high levels of NO production and its resultant metabolite, $ONOO^-$, through cytokine-induced iNOS, have an inhibitory effect on osteoblastic growth and differentiation even though NO per se has an enhancing effect. Although our data do not consider a role for eNOS as mediators of osteoblast differentiation due to focus on the iNOS pathway, eNOS mRNA expression is confirmed, at least under the experimental conditions described in this study (no data shown).

We documented previously that the marker NT was formed from $ONOO^-$ generated via NO and O_2^- after cytokine stimulation in osteoblasts, which provided a useful marker for $ONOO^-$. As expected, by immunocytochemical analysis, confirming the cellular distribution, we showed that staining levels of not only iNOS but also NT tend to decrease because of blockade of the iNOS pathway. The formation of NT is widely believed to be a result of the attack on tyrosine by $ONOO^-$ (9), but it actually may be safer to conclude that the formation of NT is a result of the generation of reactive nitrogen species rather than $ONOO^-$ specifically, because other pathways of NO/$ONOO^-$ interaction have been proposed in a previous report (26). The effects of iNOS antisense may have different aspects of osteoblast function on growth and differentiation. We showed that the indexes of osteoblastic differentiation, COL I, ALPase, OSC, and Cbfa1, were upregulated in the antisense cell lines with cytokines. However, iNOS antisense only partially attenuated the reduction of

proliferation in the presence of cytokines. These data seemed to suggest that iNOS antisense had a more profound effect of osteoblast differentiation than proliferation.

In conclusion, it was likely that the iNOS antisense-transfected cell lines, derived from osteoblastic MC3T3-E1 cells, produced substantially less NO and $ONOO^-$ after cytokine stimulation and also that the indirect inhibition of $ONOO^-$ and its cytotoxic effects resulted in the prevention of osteoblastic dysfunction. Further studies must be done to quantify this association. A recent study (11) also shows that inflammatory cytokines can indirectly induce $ONOO^-$ production and that $ONOO^-$ is at least partially responsible for proliferation and differentiation in human osteoblasts by pharmacological manipulation, which is also suggested in our studies (20, 21).

A large amount of NO derived from iNOS and tyrosine nitration has been detected in chronic inflammatory lesions (22, 44). In these pathological situations, blockade of the iNOS pathway by antisense may terminate the process of bone resorption. Therefore, targeting of iNOS with antisense DNA plasmid, although it is necessary to use higher transfection technologies such as a virus vector, may be potentially applicable to inflammatory conditions and supply therapeutic strategies for arthritis, periodontitis, and other pathological processes in inflammatory conditions.

We thank Dr. Mitsuhiro Kuwahara and Akiko Kurachi (University of Michigan) for critical reading of the manuscript.

DISCLOSURES

This work was financially supported by a grant-in-aid from the Ministry of Education, Culture, Science, Sports and Technology, the Ministry of Health, Welfare and Labor in Japan, Uehara Memorial Foundation, and the Motor Vehicle Foundation.

REFERENCES

1. **Armour KE, Armour KJ, Gallagher ME, Godeche A, Helfrich MH, Reid DM, and Ralston SH.** Defective bone formation and anabolic response to exogenous estrogen in mice with targeted disruption of endothelial nitric oxide synthase. *Endocrinology* 142: 760–766, 2001.
2. **Armour KE, van't Hof RJ, Grabowski PS, Reid DM, and Ralston SH.** Evidence for a pathogenic role of nitric oxide in inflammation-induced osteoporosis. *J Bone Miner Res* 14: 2137–2142, 1999.
3. **Armour KJ, Armour KE, van't Hof RJ, Reid DM, Wei XQ, Liew FY, and Ralston SH.** Activation of the inducible nitric oxide synthase pathway contributes to inflammation-induced osteoporosis by suppressing bone formation and causing osteoblast apoptosis. *Arthritis Rheum* 44: 2790–2796, 2001.
4. **Bertolini DR, Nedwin GE, Bringman TS, Smith DD, and Mundy GR.** Stimulation of bone resorption and inhibition in vitro. *Nature* 319: 516–518, 1986.
5. **Bogle RG, Macallister RJ, Whitley GS, and Vallance P.** Induction of N^G-monomethyl-L-arginine uptake: a mechanism for differential inhibition of NO synthase. *Am J Physiol Cell Physiol* 269: C750–C756, 1995.
6. **Brandi ML, Hukkanen M, Umeda T, Moradi-Bidhendi N, Bianchi S, Gross SS, and Polak JM.** Bidirectional regulation of osteoclast function by nitric oxide synthase isoforms. *Proc Natl Acad Sci USA* 92: 2954–2958, 1995.
7. **Cartwright JE, Johnstone AP, and Whitley GS.** Inhibition of nitric oxide synthase by antisense techniques: investigations of the roles of NO produced by murine macrophage. *Br J Pharmacol* 120: 146–152, 1997.
8. **Cartwright JE, Johnstone AP, and Whitley GS.** Endogenously produced nitric oxide inhibits endothelial cell lines. *Br J Pharmacol* 131: 131–137, 2000.
9. **Crow JP and Ischiropoulos S.** Detection and quantitation of nitrotyrosine residues in proteins: in vitro marker of peroxynitrite. *Methods Enzymol* 269: 185–194, 1996.
10. **Damoulis PD and Hauschka PV.** Cytokines induce nitric oxide production in mouse osteoblasts. *Biochem Biophys Res Commun* 201: 924–931, 1994.
11. **Da Rocha FAC and de Brum-Fernandes AJ.** Evidence that peroxynitrite affects human osteoblast proliferation and differentiation. *J Bone Miner Res* 17: 434–442, 2002.
12. **Dawson TM, Bredt DS, Fotuhi M, Hwang PM, and Snyder SH.** Nitric oxide synthase and neuronal NADPH diaphorase are identical in brain and peripheral tissues. *Proc Natl Acad Sci USA* 88: 7797–7801, 1991.
13. **Deodhar AA and Woolf AD.** Bone mass measurement and bone metabolism in rheumatoid arthritis: a review. *Br J Rheumatol* 35: 309–322, 1996.
14. **Evans DB, Thavarajah M, and Kanis JA.** Involvement of prostaglandin E_2 in the inhibition of osteocalcin synthesis by human osteoblast-like calls in response to cytokines and systemic hormones. *Biochem Biophys Res Commun* 167: 194–202, 1990.
15. **Farrell AJ, Blake DR, Palmer RM, and Moncada S.** Increased concentrations of nitrite in synovial fluid and serum samples suggest increased nitric oxide synthesis in rheumatic diseases. *Ann Rheum Dis* 51: 1219–1222, 1992.
16. **Garvey EP, Oplinger JA, Furfine ES, Kiff RJ, Laszlo F, Whittle BJ, and Knowles RG.** 1400 W is a slow, tight binding, and highly selective inhibitor of inducible nitric-oxide synthase in vitro and in vivo. *J Biol Chem* 272: 4959–4963, 1997.
17. **Gewirtz AM, Stein CA, and Glazer PM.** Facilitating oligonucleotide delivery: helping antisense deliver on its promise. *Proc Natl Acad Sci USA* 93: 3161–3163, 1996.
18. **Grabowski PS, England AJ, Dykhuizen R, Copland M, Benjamin N, Reid DM, and Ralston SH.** Elevated nitric oxide production in rheumatoid arthritis. *Arthritis Rheum* 39: 643–647, 1996.
19. **Green LC, Wangner DA, Glogowski J, Skipper PL, Wishnok JS, and Tannenbaum SR.** Analysis of nitrate, nitrite, and [^{15}N]nitrate in biological fluids. *Anal Biochem* 126: 131–138, 1982.
20. **Hikiji H, Shin WS, Koizumi T, Takato T, Susami T, Koizumi Y, Okai-Matsuo Y, and Toyo-oka T.** Peroxynitrite production by TNF-α and IL-1β: implication for suppression of osteoblastic differentiation. *Am J Physiol Endocrinol Metab* 278: E1031–E1037, 2000.
21. **Hikiji H, Shin WS, Oida S, Takato T, Koizumi T, and Toyo-oka T.** Direct action of nitric oxide on osteoblastic differentiation. *FEBS Lett* 410: 238–242, 1997.
22. **Hilliquin P, Borderie D, Hernvann A, Menkes CJ, and Ekindjian O.** Detection of nitric-oxide complexed in s-nitrosoproteins in rheumatoid-arthritis (ra) (Abstract). *Arthritis Rheum* 39: 320, 1996.
23. **Hoque AM, Papapetropoulos A, Venema RC, Catravas JD, and Fuchs L.** Effects of antisense oligonucleotide to iNOS on hemodynamic and vascular changes induced by LPS. *Am J Physiol Heart Circ Physiol* 275: H1078–H1083, 1998.
24. **Hukkanen M, Hughes FJ, Buttery LDK, Gross SS, Evans TJ, Seddon S, Riveros-Moreno V, Macintyre I, and Polak JM.** Cytokine-stimulated expression of inducible nitric oxide synthase by mouse, rat, human osteoblast-like cells and its functional role in osteoblast metabolic activity. *Endocrinology* 136: 5445–5453, 1995.
25. **Krieg AM, Yi AK, Matson S, Waldschmidt TJ, Bishop GA, Teasdale R, Koretzky GA, and Klinman DM.** CpG motifs in bacterial DNA trigger direct B-cell activation. *Nature* 374: 546–549, 1995.
26. **Kr Ncke K, Suschek CV, and Kolb-Bachofen V.** Implications of inducible nitric oxide synthase expression and enzyme activity. *Antiox Redox Signal* 2: 585–605, 2000.

27. **Lader CS and Flanagan AM.** Prostaglandin E, interleukin 1α and bone resorption in vitro. *Endocrinology* 139: 3157–3164, 1998.
28. **Lewis JG, Lin K, Kothavale A, Flanagan WM, Matteucci MD, DePrince RBB, Mook RA, Hendren RW, and Wagner RW.** A serum-resistant cytofectin for cellular delivery of antisense oligodeoxynucleotides and plasmid DNA. *Proc Natl Acad Sci USA* 93: 3176–3181, 1996.
29. **Lewis RS, Tamir S, Tannenbaum SR, and Deen WM.** Kinetic analysis of the fate of nitric oxide synthesizied by macrophages in vitro. *J Biol Chem* 270: 29350–29355, 1995.
30. **Löwik CWGM, Nibbering PH, Ruit M, and Papapoulos SE.** Inducible production of nitric oxide in osteoblast-like cells and in fatal mouse bone explants is associated with suppression of osteoclastic bone resorption. *J Clin Invest* 93: 1465–1472, 1994.
31. **Lyons CR, Orloff GJ, and Cunningham JM.** Molecular cloning and functional expression of an inducible nitric oxide synthase from a murine macrophage cell line. *J Biol Chem* 267: 6370–6374, 1992.
32. **MacIntyre I, Zaidi M, Alam ASMT, Datta HK, Moonga BS, Lidbury PS, Hecker M, and Vane J.** Osteoclastic inhibition of nitric oxide not mediated by cyclic GMP. *Proc Natl Acad Sci USA* 88: 2936–2940, 1991.
33. **McDonald KK, Zharikov S, Block ER, and Kilberg MS.** A caveolar complex between the cationic amino acid transporter 1 and endothelial nitric-oxide synthase may explain the "Arginine paradox." *J Biol Chem* 272: 31213–31216, 1997.
34. **Moncada S, Palmer RMJ, and Higgs EA.** Nitric oxide: physiology, pathophysiology and pharmacology. *Pharmacol Rev* 43: 109–142, 1991.
35. **Palmer RMJ, Ferrige AG, and Moncada S.** Nitric oxide release accounts for the biological activity of endothelium-derived relaxing factor. *Nature* 327: 524–526, 1987.
36. **Ralston SH, Ho LP, Helfrich MH, Grabowski PS, Johnston PW, and Benjamin N.** Nitric oxide: a cytokine-induced regulator of bone resorption. *J Bone Miner Res* 10: 1040–1049, 1995.
37. **Rothe H, Bosse G, Fischer HG, and Kolb H.** Generation and characterization of inducible nitric oxide synthase deficient macrophage cell lines. *Biol Chem Hoppe-Seyler* 377: 227–231, 1996.
38. **Stein CA and Cheng YC.** Antisense oligonucleotides as therapeutic agents—is the bullet really magical? *Science* 261: 1004–1012, 1993.
39. **Taichman RS and Hauschka PV.** Effects of interleukin-1β and tumor necrosis factor-α on osteoblastic expression of osteocalcin and mineralized extracellular matrix in vitro. *Inflammation* 16: 587–601, 1992.
40. **Van't Hof RJ, Armour KJ, Smith LM, Armour KE, Wei XQ, Liew FY, and Ralston SH.** Requirement of the inducible nitric oxide synthase pathway for IL-1-induced osteoclastic bone resorption. *Proc Natl Acad Sci USA* 97: 7993–7998, 2000.
41. **Van't Hof RJ and Ralston SH.** Nitric oxide and bone. *Immunology* 103: 255–261, 2001.
42. **Wagner RW and Stein CA.** The state of the art in antisense research. *Nat Med* 1: 1116–1121, 1995.
43. **Weinreb M, Shinar D, and Rodan GA.** Different pattern of alkaline phosphatase, osteopontin, and osteocalcin expression in developing rat bone visualized by in situ hybridization. *J Bone Miner Res* 5: 831–842, 1990.
44. **White CR, Brock TA, Chang L, Crapo J, Briscoe P, Ku D, Bradly WA, Gianturco SH, Gore J, Freeman BA, and Tarpey MM.** Superoxide and peroxynitrite in atherosclerosis. *Proc Natl Acad Sci USA* 91: 1044–1048, 1994.

Original Article

Effects of the Anti-Platelet Aggregation Drug Dilazep on Cognitive Function in Dahl Salt-Sensitive Rats

Atsushi NUMABE, Nusrat ARA*1, Rie HAKAMADA-TAGUCHI*2, Noriko SUZUKI, Nobuhito HIRAWA*4, Yukari KAWABATA*3, Toshiyuki NEGORO*3, Taiji NAGATA*3, Atsuo GOTO*3, Teruhiko TOYO-OKA*2, Toshiro FUJITA*3, and Yoshio UEHARA*2,3

Among the consequences of the increasing prolongation of lifespan is a worldwide increase in the number of cases of dementia or impaired cognition. In the present study, to test the hypothesis that mechanisms independent of high blood pressure are involved in maintaining cognitive function, we assessed the effects of long-term dilazep treatment on cognitive dysfunction in normotensive Dahl salt-sensitive (Dahl S) rats fed a low-salt diet, using the standard passive avoidance test. Normotensive Dahl S rats fed a 0.3% NaCl diet were treated for 6 months with low-dose dilazep (2.5 μg/ml in drinking water) or high-dose dilazep (12.5 μg/ml). Systolic blood pressure was within normotensive range throughout the study and did not differ among the experimental groups. The results of the passive avoidance test revealed that dilazep treatment attenuated the decline of latency time relative to that in the untreated control rats (control latency time, 235 s; low-dilazep group, 389 s; high-dilazep group, 397 s), suggesting that the cognitive function of normotensive Dahl S rats was improved by dilazep treatment. This improvement of cognition was associated with significant increases in the number of neuronal cells in the hippocampal region and with an increase in capillary length in dilazep-treated Dahl rats. In addition, the dilazep treatments significantly attenuated arteriolar injury of glomeruli in the kidney. These data suggest that dilazep treatment, through vascular and non-vascular effects, maintains the brain function in Dahl S rats susceptible to vascular injury and organ dysfunction.
(*Hypertens Res* 2003; 26: 185–191)

***Key Words*: Dahl rats, dilazep, cognition, blood pressure, glomerulosclerosis**

Introduction

The dramatic prolongation of human lifespan has led to a rapid increase in the population of elderly across the world. One consequence of this trend in the population distribution has been an increase in the number of elderly with dementia or impairment of cognition. High blood pressure has been well demonstrated to be a risk factor for impaired cognitive function in the elderly (*1–3*). Several long-term clinical trials have revealed that blood pressure control leads to prevention of dementia (*1*). Moreover, we have demonstrated that elderly, normotensive Dahl salt-sensitive (Dahl S) rats maintain their cognitive function when treated with long-term renin-angiotensin inhibition, and this result is associated with maintenance of capillary density in the hippocampal region (*4*). The data strongly suggest that mechanisms independent of high blood pressure, and thus independent of blood pressure control, contribute to the maintenance of cognitive function in the elderly. Dilazep, a nucleoside transporter inhibitor, was originally developed to relieve angina in ischemic heart disease, and its effects have been shown to be partly mediated by

From the Department of Clinical Laboratory Medicine and Institute of Medical Science, Dokkyo University School of Medicine, Tochigi, Japan, *1Department of Cardiology, Rawalpindi Medical School, Rawalpindi, Pakistan, *2Health Service Center and *3Department of Medicine, University of Tokyo, Tokyo, Japan, and *4Second Department of Medicine, Yokohama City University, Yokohama, Japan.
Address for Reprints: Yoshio Uehara, M.D., Health Service Center and Department of Medicine, University of Tokyo, 7–3–1 Hongo, Bunkyo-ku, Tokyo 113–0033, Japan. E-mail: uehara-2im@h.u-tokyo.ac.jp
Received August 1, 2002; Accepted in revised form October 15, 2002.

inhibition of platelet aggregation (*5*, *6*). In addition, this drug uniquely behaves *in vitro* as an oxygen-radical scavenger (*7*). Such multifactorial actions are believed to attenuate mesangial cell proliferation or glomerular injury in immunoglobulin A (IgA) nephropathy (*8–10*). More interestingly, dilazep is reported to prevent the appearance of neurological symptoms and brain damage induced by ischemia following carotid artery occlusion and reperfusion, probably through suppression of lipid peroxidation (*11*). Considering these data, it is conceivable that dilazep treatment attenuates brain dysfunction in rats with susceptibility to vascular injury through these various vascular effects.

Thus, to test the hypothesis that mechanisms independent of high blood pressure are involved in maintaining cognitive function in rats prone to vascular injury, we assessed the effects of long-term dilazep treatment on cognitive dysfunction in normotensive Dahl S rats fed a low-salt diet, using the standard passive avoidance test.

Methods

In Vivo Experiment

Four-week-old Dahl S rats ($n=42$) were purchased from Seac Yoshitomi Co., Ltd., Fukuoka, Japan. The rats had been fed a low-salt (0.3% NaCl) diet after weaning. At the age of 8 weeks, they were divided into three groups: a low-dose dilazep group given 2.5 μg/ml dilazep in drinking water ($n=14$); a high-dose dilazep group given 12.5 μg/ml dilazep in drinking water ($n=14$); and a control group given water alone ($n=14$). The drug was dissolved in a drinking water at appropriate concentrations for each group. The rats were given drinking water *ad libitum*. The doses employed in the present study have been reported to inhibit platelet aggregation in rats *in vivo* (*12*). The rats were maintained for 7 months, and their cognitive function was assessed during the final month. The procedures followed were in accordance with institutional guidelines.

Systolic blood pressure was determined by the tail-cuff method (*4*, *13*, *14*). A 24-h urine specimen was collected on three consecutive days, and the urine collected on the last day was used for determination of various parameters. Under Inaction anesthesia (75 mg/kg body weight), the right kidney was removed for morphological investigation, and then, whole blood samples and the other organs of interest were obtained.

Estimation of Learning Ability by Passive Avoidance Task

The behavioral experiments were performed in a quiet, diffusely lighted room (indirect light was provided by 25 W lamps at a height of 1.5 m above the animals). After the rats were acclimated to the room, they were trained in a conventional step-through passive avoidance apparatus divided into a light and a dark chamber. The apparatus had a stainless-steel grid floor and the chambers were separated by a slit door (*4*, *15*, *16*). Each animal was placed initially in a safe and lighted room with the slit-door closed. After 60 s of equilibrium stabilization, the slit-door to the dark chamber was opened. After the rats stepped into the dark room, the door was closed and an electric shock (75 V, 500 mA) was administered to the feet *via* the grid. After 10 s, the door was re-opened and the rats had access to the safe lighted room. The dose of electric shock was preliminarily determined according to previous studies (*4*). Through a series of these procedures, the risk and its avoidance were engraved on their memory.

To determine preservation of the memory, response latency was measured. Briefly, the shock generator was turned off and the rats were placed in the safe, lighted chamber. We then measured the time passed until they stepped into the dark chamber. In cases in which more than 400 s elapsed, the rats were considered to have completely preserved the memory.

Basic behavioral activity and movement were estimated using the open field test. Briefly, the rats were placed in a quiet and lighted room having a floor divided into 40×50 cm compartments marked by grid-lines. The rats were allowed to move freely. We then determined how many times the rat crossed the grid-lines in a 2-min period. The experiment was repeated three times, and the values were averaged to obtain a basal level of movement. This test was repeated on three successive days, and only the values of the second and third trials were used for analysis.

Morphological Study of the CA1 Hippocampal Region

The whole brain was embedded in paraffin with the cerebrum. Five-micrometer serial sections in the CA1 hippocampal region were stained with Bodian and Reticulin. Neurons in the zone of the CA1 region next to the CA2 were counted under an Olympus model BX 51 light microscope (Olympus, Tokyo, Japan) equipped with a computer-assisted digital image analyzer (DP-50; Olympus). The total for three areas was averaged to obtain the cell number of neuronal cells in this zone. For comparison, we measured the cell number in the cortical region using the same procedures as for the hippocampal region.

In order to determine the vascular density in the CA1 region, we measured the length of capillaries in the hippocampus area using the light microscope system and quantitative image analyzing application (WinRoof; Mitani Corp., Tokyo, Japan). The values in 6 continuous areas were averaged to obtain the capillary density. For comparison, we measured capillary density in the cortex using the same method.

Measurement of Lipid Peroxides

To assess the antioxidant effects of dilazep, we measured plasma and urinary concentrations of lipid peroxides as malon-

Table 1. Organ Weights in Dahl S Rats

Group	CONT (n=10)	DIL-LOW (n=13)	DIL-HIGH (n=12)	p values*
BW (g)	511.4±17.5	473.3±18.0	497.8±11.4	NS
Heart weight (g/kg BW)	3.70±0.16	3.95±0.21	3.68±0.11	NS
Kidney weight (g/kg BW)	5.87±0.21	5.98±0.29	6.05±0.14	NS

BW, body weight; CONT, Dahl S rats fed a low-salt diet alone; DIL-LOW, rats given a low-dose of dilazep; DIL-HIGH, rats given a high-dose of dilazep. * As assessed by one-way ANOVA; NS, not statistically significant.

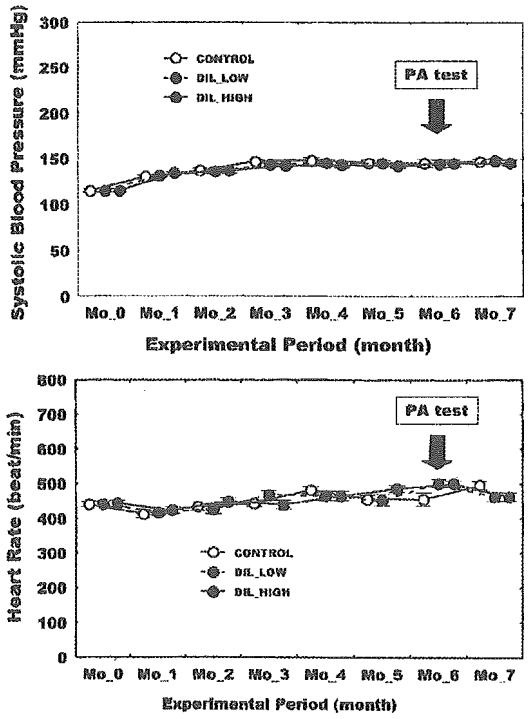

Fig. 1. *Time-dependent alterations in systolic blood pressure and heart rate. Eight-week-old Dahl S rats were fed a low-salt diet. The passive avoidance task test (PA test) was done at month 6 and the cognitive function was followed up for another 1 month. CONT, Dahl S rats fed a low-salt diet alone (n=10); DIL-LOW, 13 rats given a low-dose of dilazep (n=13); and DIL-HIGH, rats given a high-dose of dilazep (n=12). There were no differences in blood pressure levels or heart rate among the three experimental groups.*

dialdehyde (MDA), an endproduct of lipid peroxides, according to the method previously reported (*17*). Briefly, 1 ml plasma or urine was mixed with 5 ml of 20% trichloracetic acid and vigorously vortexed. The mixture was incubated at 4°C for 30 min and then was centrifuged at 2,000×g at 4°C for 15 min. Two milliliters of the supernatant was heat-treated at 100°C for 15 min with 0.4 ml of 0.12 mol/l thiobarbituric acid solutions at pH 7.4. The optical absorbance of MDA was measured at 532 nm by a Hitachi U-3200 spectrophotometer (Hitachi Ltd., Tokyo, Japan). MDA in media prior to the assay (zero time incubation) was determined so that the net MDA production during the reaction could be measured.

Functional and Morphological Alterations of the Kidney

To assess renal function, we determined plasma and urinary levels of creatinine, plasma levels of electrolytes, and urinary protein excretions as reported previously (*4*, *13*, *14*, *17*).

Glomerular lesions in the kidney were assessed according to the method described in previous studies (*4*, *13*, *14*, *17*). The severity of these lesions was graded. An overall glomerulosclerosis score (GS) was obtained by multiplying the severity score by the percentage of glomeruli displaying the same degree of injury and adding these scores. Theoretically, the GS ranges from 0 (intact glomeruli only) to 400 (all glomeruli showing obsolescence).

To assess the collagen accumulation in the outer medulla, we utilized RGB color analysis of collagen fibrils stained by Azan and determined the area showing the same pattern of RGB wavelength as the collagen fibrils using an Olympus microscope and WinRoof color analyzing software (Mitani Corp.). The measurements were expressed as the percentage of collagen to the whole area tested.

Statistical Analysis

Values are expressed as the means±SEM. Differences were analyzed by one-way analysis of variance (ANOVA) and Duncan's multiple range tests or two-way ANOVA followed by *post hoc* Scheffe's multiple comparison using the STATISTICA program (StatSoft, Tulsa, USA). Values of $p<0.05$ were considered to indicate statistical significance.

Results

Hemodynamics

Before the assessment of cognitive function, 4 rats in the untreated group, 1 rat in the low-dose group and 2 rats in the high-dose group died of renal failure. The data for the remaining 35 rats were used for the present analysis. The averaged amounts of water consumed were 35.1±3.2 ml/day for the low-dose group, 40.5±5.4 ml/day for the high-dose

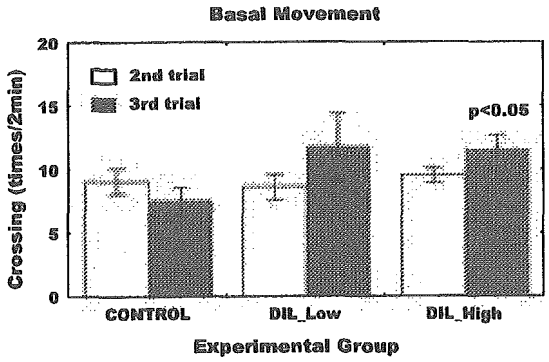

Fig. 2. *Effects of dilazep on basal movement of Dahl S rats. The effects of dilazep on basal movement are shown. CONT, Dahl S rats fed a low-salt diet alone (n=10); DIL-LOW, rats given a low-dose of dilazep (n=13); and DIL-HIGH, rats given a high-dose of dilazep (n=12). The experiment was repeated three times. The values were averaged to obtain the measurement of the basal movement. This test was repeated on three successive days, and the values on the second and third trials were analyzed in the present study. Differences among groups were assessed by one-way ANOVA.*

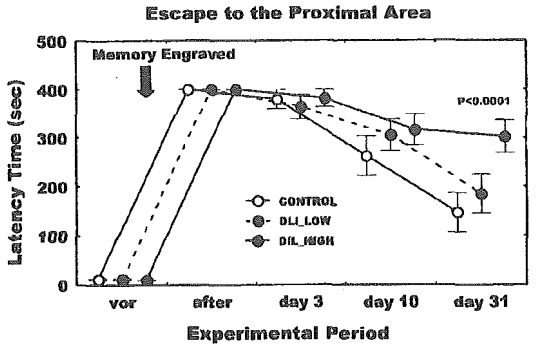

Fig. 3. *Effects of dilazep on response latency in the step-through passive avoidance task. The response latency was assessed at Days 1, 3, 10 and 31 after the engraving of the memory. The maximum latency was assessed as 400 s. The response latency was time-dependently decreased after electric shock. CONT, Dahl S rats fed a low-salt diet alone (n=10); DIL-LOW, rats given a low-dose of dilazep (n=13); and DIL-HIGH, rats given a high-dose of dilazep (n=12). The differences were analyzed using two-way ANOVA and* post hoc *Scheffe's multiple comparison. The group and time differences were $p<0.05$ and $p<0.0001$, respectively. There was a significant difference between the high-dose and control groups (Scheffe's test, $p<0.05$). Similarly, the time dependency was assessed and there were significant differences between the response latency values immediately after the stimulation and at each of Days 10 and 31 ($p<0.0001$, $p<0.0001$, respectively). One-way ANOVA, as indicated by p value in the graph, was used to compare the difference in response latency at Day 31 between the high-dose and control groups.*

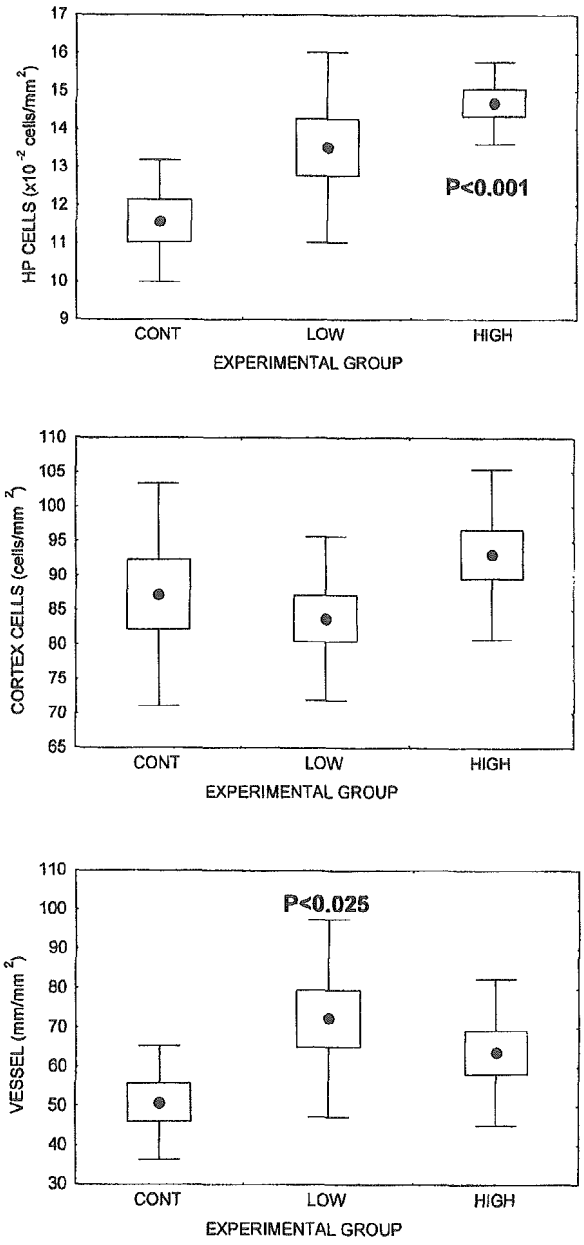

Fig. 4. *Neuronal cells and capillaries in the hippocampal region in dilazep-treated rats. CONT, Dahl S rats fed a low-salt diet alone (n=10); LOW, rats given a low-dose of dilazep (n=13); and HIGH, rats given a high-dose of dilazep (n=12). The number of cells in the CA1 hippocampal area is shown in upper graph, the number of cells in the cerebral cortex is shown in the middle graph, and the vessel density is shown in the lower graph. The measurements were compared with the values in CONT. Differences among groups were assessed by one-way ANOVA.*

Table 2. Effects of Dilazep on Renal Function in Dahl S Rat

Variables	Unit	CONT ($n=10$)	DIL-LOW ($n=13$)	DIL-HIGH ($n=12$)
Na	mEq/l	153.7±1.3	155.6±2.1	151.8±3.9
K	mEq/l	4.39±0.14	4.64±0.24	4.67±0.21
Cr	mg/dl	2.17±0.34	2.53±0.44	1.82±0.20
Uprotein	mg/day	234.3±4.2	220.3±20.9	238.9±21.2
Ccr	ml/day	9.653±1.311	10.048±1.943	9.695±1.035
pMDA	ng/ml	0.3125±0.0109	0.3705±0.0318	0.2786±0.0232
uMDA	nmol/day	2.9232±0.7063	5.8155±1.1335	3.5378±0.9233
GS score	arbitrary	281±20	275±13	229±9*
Collagen	%	0.0814±0.0085	0.0877±0.0131	0.0755±0.0080

Na, plasma Na concentration; K, plasma K concentration; Cr, plasma creatinine concentration; Uprotein, urinary protein excretion; Ccr, creatinine clearance; pMDA, plasma malondialdehyde concentration; uMDA, urinary malondialdehyde excretion; GS score, glomerular sclerosis score; Collagen, area of collagen infiltration in the renal medulla; CONT, Dahl S rats fed a low-salt diet alone; DIL-LOW, rats given a low-dose of dilazep; DIL-HIGH, rats given a high-dose of dilazep. GS score ranges from 0 (intact glomeruli only) to 400 (all glomeruli showing obsolescence). * $p<0.025$ *vs.* CONT. Differences among groups were assessed by one-way ANOVA followed by Duncan's multiple range test.

group, and 36.9±2.5 ml/day for the control group. Based on these data, the dilazep dosages were 0.16±0.01 and 0.94± 0.12 mg/kg body weight per day for the low-dose and high-dose dilazep groups, respectively. The doses of dilazep used in the present study were well within the therapeutic range for anti-platelet aggregation.

The systolic blood pressure gradually increased with age in each of the three groups (Fig. 1). However, the blood pressures were within the normotensive range throughout the study, and were not significantly different among the three groups. Similarly, there were no differences in heart rate, body weight, heart weight or kidney weight among the three groups (Table 1).

Behavior and Learning Ability

First, we checked the effects of the treatments on the behavior of the rats. Basic behavioral activity and movement were assessed using the open-field test according to the method of Braszko and Wisniewski (*15*). In the second trial of the frequency of crossing in the open-field, there was no statistical difference; however, in the third trial, the high-dose dilazep treatment significantly improved the basal movement, as compared with the control group (Fig. 2). This clearly suggested that the high-dose dilazep treatment improved the searching ability and basic movements.

The response latency values in the step-through passive avoidance task, a useful index of learning ability, are demonstrated in Fig. 3. The differences were analyzed using two-way ANOVA and by *post hoc* Scheffe's multiple comparison. The group and time differences were statistically significant ($p<0.05$ and $p<0.0001$, respectively). The difference in response latency values between the high-dose dilazep and control groups was also statistically significant (Scheffe's test, $p<0.05$). Similarly, the time dependency was assessed by Scheffe's test and there was a significant difference between the values after the stimulation and those on Day 10 or Day 31 (Scheffe's test, $p<0.0001$, $p<0.0001$). One-way ANOVA, as indicated by p value in the graph, was used to compare the difference in response latency at Day 31 between the high-dose and control groups. Thirty-one days after electric shock, the latency of the untreated control rats averaged 235±50 s. However, the dilazep treatment preserved latency up to 389±11 s for the low-dose dilazep group and 397±3 s for the high-dose dilazep group ($p<0.001$ *vs.* the untreated control group), suggesting that the dilazep treatment significantly sustained cognitive function.

Next, we determined the number of neuronal cells in the hippocampal region (Fig. 4). Both the number of neurons in the low-dose group (1,276±151 cells/mm^2) and that in the high-dose group (1,432±73 cells/mm^2) were significantly higher than that in the control group (1,102±113 cells/mm^2) ($p<0.01$, respectively). In contrast, there were no differences in the cell number in the cerebral cortex among the three groups. We determined the total length of capillaries in a given area of the CA1 region of hippocampus. The total length of capillaries in the hippocampal area tended to be higher in the dilazep-treatment groups than in the controls, and particularly in the low-dose group, where the length was approximately 42% longer than that in the control group (50.8±4.8 *vs.* 72.3±1.1 mm/mm^2, $p<0.025$). We also measured capillary length in the cortex using the same method. The capillary density was 1,418±90 pm/μm^2 for the control group, 1,454± 168 pm/μm^2 for the low-dose dilazep group and 1,664±99 pm/μm^2 for the high-dose dilazep group. There were no significant differences among the three groups.

Kidney Function

We also investigated the effects of dilazep treatment on kid-

ney function (Table 2). The dilazep treatments did not significantly affect the plasma or renal variables used as indices of renal function. Although high-dose dilazep treatment tended to decrease plasma MDA concentrations, this difference did not reach the level of statistical significance. Similarly, urinary MDA excretions were not influenced by the dilazep treatments. In contrast, the high-dose treatment significantly attenuated the glomerular sclerosis index, as compared with that in the untreated group. Similarly, collagen accumulation in the renal medulla tended to decline in the high-dose group, but this difference was not statistically significant.

Discussion

To assess learning ability, we performed a passive avoidance test according to the standard method described previously (*4*, *15*, *16*). This is an established test to assess memory function in the field of behavioral pharmacology. Latency time, the time required to re-enter the dark room, is influenced essentially by the basic movement of animals and their learning ability. We demonstrated in the present study that the basal movement was higher in the dilazep-treated groups than in the control rats, and this increase would be expected to promote a decrease in latency time, and thus in cognitive function. However, we demonstrated that the latency time actually increased in the dilazep-treated rats, as compared with the control rats, thereby suggesting that dilazep treatment improved cognitive function in Dahl S rats fed a low-salt diet. These data indicated that the latency time determined in the present study reflected the learning ability of the rats and was not due to alterations of the basal movement.

More intriguingly, the maintenance of cognitive function observed in the dilazep-treatment groups was associated with preservation of neural cells and capillary density in the CA1 hippocampal region. The precise mechanism by which dilazep treatment preserved cognitive function is not clear at this time. Cognition is formed by a network that includes the sensory organs, neural functions in the hippocampus, amygdala and hypothalamus, and subsequent integration of the information in the brain. Within this network, the hippocampus is considered the gateway to memory. The CA1 hippocampal region in particular is one of the most important areas for cognitive function, and is noted for its susceptibility to ischemia (*18*, *19*). Sakanaka *et al.* have demonstrated that there is a relationship between the latency of the passive avoidance task and the cell density of the CA1 region (*20*). Our present results on the cerebral function and morphological changes of the brain are in accordance with these previous study (*4*, *18–20*). Such a structural difference in the vascular system may explain the difference in neuronal cell preservation between the CA1 region and the deep cortex. The preservation of the neuronal cells and vascular density in this particular region is presumed to be critical for the dilazep-induced maintenance of cognitive function.

In this context, we have previously reported that an angiotensin converting enzyme inhibitor (ACEI) attenuated the aged-related decline of cognitive function in elderly Dahl S rats with normal blood pressure (*4*). This benefit was associated with the maintenance of capillary density and neural cells in the CA1 hippocampal region. More intriguingly, it is achieved only by long-term treatment, and not by short-term treatment. Similarly, in their study on elderly hypertensive patients, Leonetti and Dalvetti reported that 12-week treatment with an ACEI or calcium channel blocker was not effective at improving memory function (*2*). These data indicate that the preservation of cognition by dilazep treatment was due to protection of the vascular vessels responsible for sustaining the neural cells in the hippocampus area rather than acute effects like blood pressure reduction. In this context, we demonstrated that dilazep treatment indeed attenuated glomerular sclerosis, suggesting that the vascular protection was observed throughout the systemic circulation. In addition, it has been well documented that dilazep, a nucleoside transporter inhibitor, behaves as an anti-platelet aggregatory drug and an oxygen-radical scavenger, and prevents the appearance of neurological symptoms and brain damage induced by ischemia and reperfusion (*5–11*). Unfortunately, we were unable to provide evidence that the scavenging effects of dilazep participated in the preservation of cognition. Dilazep is known to exert its scavenging action on local lesions in the brain and kidney, and seemingly, MDA in plasma and urine might not reflect the reduction/oxidation (REDOX) mechanism underlying the organ damage. If this is true, we cannot rule out the possible involvement of the REDOX phenomenon, and we might better investigate the tissue MDA formation to assess the scavenging effects of dilazep treatment. Taken together, the results indicate that these vascular and non-vascular effects of dilazep are integrated to maintain the brain function in Dahl S rats susceptible to vascular and organ injury.

There has been increasing interest in the effects of antihypertensive treatment on cognitive dysfunction or dementia in the elderly. Long-term treatment with nitrendipine alone or in combination with an ACEI or a diuretic reduces the incidence of an Alzheimer-type dementia by about 50% (*1*). Very recently, similar effects have been reported by treatment with amlodipine (*21*). Blood pressure reduction *per se* contributes to the prevention of dementia in hypertension. Interestingly, in our previous study, we demonstrated that even in the normotensive Dahl S rats, blood pressure values independently contribute to determining the preservation of neuronal cells in the hippocampal area, thereby suggesting that rising blood pressure within the normotensive range along with aging are risk factors for age-related vascular injuries and subsequent organ damage (*4*). In addition, a recent clinical study has demonstrated that systolic blood pressure in the normotensive range may be a risk factor for cognitive dysfunction in middle-aged, normotensive women (*3*). Thus, we cannot overemphasize the role of blood pressure in sus-

taining cognitive function. In addition, it seems worthwhile to note that mechanisms independent of blood pressure participate in sustaining cognitive function, as shown in the dilazep treatments. Various approaches to vascular protection would provide a useful strategy to prevent the coming increase in the elderly population with cognitive dysfunction.

Finally, in our study, we employed the standard passive avoidance test to assess cognitive function of Dahl S rats. Cognition is a complicated function into which many components are integrated, including sensory function, motor ability, high-level brain function and the hippocampus/amygdala/hypothalamus system. In animal studies, there are limitations in the methodology for assessing whole cognitive function. In this sense, it should be noted that the passive avoidance test assesses only a portion of overall cognition, as do other task tests, such as the water maze task by Morris or the T- and Y-shaped maze tests (*22*). Meticulous investigation using a behavioral pharmacological approach will be needed to draw a definite conclusion regarding the effects of dilazep on human cognition.

Acnowledgements

The authors acknowledge Kowa Pharmaceutical Co., Tokyo, Japan for their gift of dilazep.

References

1. Staessen JA, Fagard R, Thijs L, *et al*: Randomised double-blind comparison of placebo and active treatment for older patients with isolated systolic hypertension. *Lancet* 1997; **350**: 757–764.
2. Leonetti G, Dalvetti A: Effects of cilazapril and nitrendipine on blood pressure, mood, sleep, and cognitive function in elderly hypertensive patients: an Italian Multicenter Study. *J Cardiovasc Pharmacol* 1994; **24** (Suppl 3): S73–S77.
3. Hakamada-Taguchi R, Uehara Y, Negoro H, Toyo-oka T: The relationship between lower systolic blood pressure and cognitive function in normotensive, middle-aged healthy women. *Hypertens Res* 2002; **25**: 565–569.
4. Hirawa N, Uehara Y, Kawabata Y, *et al*: Long-term inhibition of renin-angiotensin system sustains memory function in aged Dahl rats. *Hypertension* 1999; **34**: 496–502.
5. Hoque AN, Hoque N, Hara A, Hashizume H, Ichihara K, Abiko Y: Cardioprotective effect of K-7259, a novel dilazep derivative, against ischemia-reperfusion damage in isolated, working rat hearts. *Jpn J Pharmacol* 1997; **73**: 365–369.
6. Ozaki Y, Jinnai Y, Yatomi Y, Tawata M, Onaya T, Kume S: Effects of dilazep on platelet functions and volume change in patients with diabetes mellitus. *Arzneimittelforschung* 1993; **43**: 536–539.
7. Asanuma A, Yamauchi Y, Koga T, Katayama I: Suppression of age-related changes in mouse hippocampal CA3 nerve cells by a free radical scavenger. *Mech Ageing Dev* 1995; **83**: 55–64.
8. Hayashi T, Kaneko S, Thang NT, Shou I, Shirato I, Tomino Y: Effect of dilazep hydrochloride on the immunohistopathology of IgA nephropathy in ddY mice. *Nephron* 2000; **86**: 327–332.
9. Gohda T, Makita Y, Shike T, *et al*: Effect of dilazep hydrochloride, an antiplatelet agent, on the proliferation of cultured mouse glomerular mesangial cells. *Nephron* 2000; **84**: 90–91.
10. Sakumura T, Fujii Z, Umemoto S, *et al*: Dilazep, a nucleoside transporter inhibitor, modulates cell cycle progression and DNA synthesis in rat mesangial cells *in vitro*. *Cell Prolif* 2000; **33**: 19–28.
11. Yamauchi Y, Ikuta J, Shimizu S, Nakamura M: Effect of dilazep dihydrochloride on ischemia and reperfusion-induced cerebral injury in spontaneously hypertensive rats. *Nippon Yakurigaku Zasshi* 1990; **95**: 239–246 (in Japanese).
12. Valori VM, Leone G, Traisci G, Bizzi B: A comparative study on the effect of dilazep and dipyridamole on some platelet functions. *Arzneimittelforschung* 1982; **32**: 403–405.
13. Hirawa N, Uehara Y, Kawabata Y, *et al*: Subpressor dose of angiotensin II increases susceptibility to the haemodynamic injury of blood pressure in Dahl salt-sensitive rats. *J Hypertens* 1995; **13**: 81–90.
14. Hirawa N, Uehara Y, Kawabata Y, *et al*: Mechanistic analysis of renal protection by angiotensin converting enzyme inhibitor in Dahl salt-sensitive rats. *J Hypertens* 1994; **12**: 909–918.
15. Braszko JJ, Wisniewski K: Effects of angiotensin II and saralasin on motor activity and the passive avoidance behavior of rats. *Peptides* 1988; **9**: 475–479.
16. Tadokoro S, Kuribara H, Hayashi H: Methodological problems on learning and memory tests in rodents from view points of behavioral toxicology, in Fujii T and Adams PM (eds): Functional Teratogenesis; Functional Effects on the Offspring after Parenteral Drug Exposure. Tokyo, Teikyo University Press, 1987, pp 53–70.
17. Uehara Y, Kawabata Y, Shirahase H, *et al*: Radical scavengers of indapamide and renal protection in Dahl salt sensitive rats. *Hypertens Res* 1992; **15**: 17–26.
18. Zola-Morgans, Squire LR, Amaral DG: Human amnesia and the medial temporal region: enduring memory impairment following a bilateral lesion limited to field CA1 of the hippocampus. *J Neurosci* 1986; **6**: 2950–2967.
19. Tabuchi E, Endo S, Ono T, Nishijo H, Kuza S, Kogure K: Hippocampal neuronal damage after transient forebrain ischemia in monkeys. *Brain Res Bull* 1992; **29**: 685–690.
20. Sakanaka M, Wen TC, Matsuda S, Morishita E, Nagao M, Sasaki R: *In vivo* evidence that erythropoietin protects neurons from ischemic damage. *Proc Natl Acad Sci U S A* 1998; **95**: 4635–4640.
21. Testa MA, Turner RP, Simonson DC, Krafcik MB, Calvo C, Luque-Otero M, the Nifedipine GITS Study Group: Quality of life and calcium channel blockade with nifedipine GITS *versus* amlodipine in hypertensive patients in Spain. *J Hypertens* 1998; **16**: 1839–1847.
22. Morris R: Developments of a water-maze procedure for studying spatial learning in the rat. *J Neurosci Methods* 1984; **11**: 47–60.

Sarcolemmal fragility secondary to the degradation of dystrophin in dilated cardiomyopathy, as estimated by electron microscopy

Tomie Kawada PhD[1], Chieko Hemmi[2], Satoru Fukuda PhD[3], Asaki Tezuka[2], Kuniaki Iwasawa MD PhD[2], Mikio Nakazawa PhD[4], Hiroshi Sato PhD[1], Teruhiko Toyo-oka MD PhD[2]

T Kawada, C Hemmi, S Fukuda, et al. Sarcolemmal fragility secondary to the degradation of dystrophin in dilated cardiomyopathy, as estimated by electron microscopy. Exp Clin Cardiol 2003;8(2):67-70.

A common gene deletion or mutation of *delta-sarcoglycan* (δ-SG) in dystrophin-related proteins (DRPs) is identified in both TO-2 strain hamsters and human families with dilated cardiomyopathy. We have succeeded in the long-lasting in vivo supplementation of a normal δ-SG gene by recombinant adeno-associated virus vector, restoration of the morphological and functional degeneration, and improvement in the prognosis of the TO-2 hamster. To evaluate the integrity of the sarcolemma (SL) and the subsequent change of organelles in cardiomyocytes of the TO-2 strain hamster, we examined electron microscopy (EM) images focusing on the sarcolemmal stability at the end stage of heart failure. Two types of sarcolemmal degradation were detected: the widened and locally thickened SL, and blurred and discontinuous SL. Bizarrely formed mitochondria of varying sizes were also observed. Immuno-EM revealed clear expression of dystrophin in the SL and intense expression at the costamere as well as at the T-tubules in the control F1B strain hearts, but a patchy deposition of dystrophin was observed along the SL without the transgene of δ-SG. In contrast to the previous reports that dystrophin's integrity was intact, the present results suggest that the gene deletion of δ-SG and the loss of δ-SG protein in the SL cardioselectively cause the morphological and functional deterioration of dystrophin and the resultant instability of the SL. The sarcolemmal fragility may be similar to Duchenne-type progressive muscular dystrophy in skeletal muscle. In addition to the mechanical role, another aspect of DRPs for the intracellular signal transmission is also discussed.

Key Words: Delta-sarcoglycan; *Dilated cardiomyopathy; Dystrophin; Dystrophin-related proteins; Gene defect; Immuno-electron microscopy; Sarcolemma; TO-2 hamster*

The pathological process of dilated cardiomyopathy (DCM) to the advanced stage is of great importance for developing both the prevention and the treatment of heart failure. A cardiomyopathic hamster is a representative model of human hereditary cardiomyopathy (CM) (1). We have identified a gene defect of *delta-sarcoglycan* (δ-SG), a component of dystrophin-related proteins (DRPs) (Figure 1), in both the BIO-14.6 strain, which shows hypertrophic CM followed by DCM, and the TO-2 strain, which reveals DCM from the onset (1-3). This δ-SG gene defect has also been reported in four human families with DCM and sudden death (4). The gene abnormality and the corresponding transgene disruption in DRPs may commonly induce muscle degeneration, especially in the sarcolemma (SL), because DRPs link intracellular contractile machinery, F-actin, with the extracellular matrix, laminin alpha-2, via dystrophin. In addition to the major role of stabilizing the SL during the repeated heart beating (Figure 1) (5), DRPs are now presumed to have another function of transmitting a mechanical stimulus to an intracellular signal.

Although many pathohistological studies have been performed in cardiomyopathic hamster hearts (1,6-8), no report has addressed the SL except our results using immunohistological analyses (3,9,10). In the present study, to evaluate the integrity of the SL and the morphological change of organelles in cardiomyocytes of TO-2 strain hamsters, we examined the fine architecture at the end stage of heart failure with conventional electron microscopy (EM). Furthermore, we focused on the exact location of δ-SG and dystrophin using an immuno-EM.

MATERIALS AND METHODS

Hereditary cardiomyopathic hamsters

TO-2 strain hamsters with hereditary DCM were used as the DCM model at age 25 weeks, when clinical symptoms of advanced heart failure became evident (3,9,10). The age-matched F1B strain hamsters were used as controls. Both male strains were purchased from Bio Breeder (Fitchburg, USA) and kept in the Infection Research Laboratory under conditions following the Japanese Pharmacological Society's *Guidance for Animal Facility*.

EM

The hamsters were deeply anesthetized with intraperitoneal injections of sodium pentobarbital (Dainippon Pharmaceutical Co, Osaka, Japan). The hearts were carefully removed and the apex was excised for EM, as described previously (11). Myocardial cubes of 1 mm were prefixed with 2.5% of glutalaldehyde in 0.1 M sodium cacodylate buffer (pH 7.4), postfixed with 1% osmium

[1]*Division of Pharmacy, Niigata University of Medical Hospital, Niigata University School of Medicine, Niigata, Japan;* [2]*Department of Pathophysiology and Internal Medicine, University of Tokyo, Tokyo, Japan;* [3]*Deparment of Pathology, Tokyo University Hospital, Tokyo, Japan;* [4]*Department of Medical Technology, Niigata University School of Medicine, Niigata, Japan*

Correspondence and reprints: Dr Tomie Kawada, Division of Pharmacy, Niigata University Medical Hospital, Asahimachidori, 1-754, Niigata 951-8520, Japan. Telephone/fax 81-25-227-2791, e-mail tomie@med.niigata-u.ac.jp

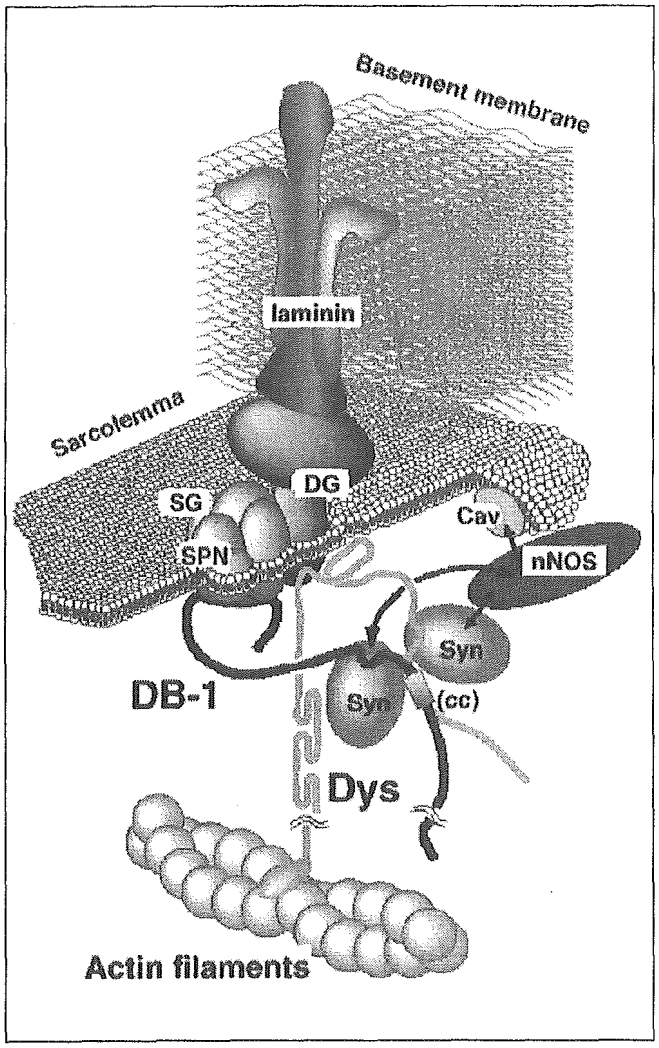

Figure 1) *A scheme of dystrophin-related proteins (DRPs). DRP is made of a protein complex consisting of alpha- and beta-dystroglycans (DG); alpha-, beta-, gamma- and delta-sarcoglycans (SG); sarcospan (SPN); and syntrophin (Syn). Note that the complex connects with the intracellular contractile machinery actin via dystrophin (Dys) and with the basement membrane at the extracellular matrix via laminin alpha-2 in addition to neuronal nitric oxide synthase (nNOS) and caveolin (Cav). This illustration was kindly presented by Dr M Yoshida, Department of Cell Biology, National Institute of Neuroscience, National Center of Neurology and Psychiatry, Japan. DB-1 Dystrobrevin-1*

tetroxide and dehydrated in graded alcohol. The tissue was embedded in Epon mixture (Resolution Performance Products, USA), and ultra-thin sections (60 nm thick) were made with an ultramicrotome (Porter-Blum MT-II, Sorvall, USA). The sections were double-stained on copper grids with uranyl acetate for 10 min to 15 min and lead nitrate for 5 min at room temperature. Sections were photographed on an electron microscope (Hitachi H-7000, Tokyo, Japan) in a magnification range from ×5000 to ×25,000.

Immuno-EM

The hearts were excised and fixed with 2% paraformaldehyde in saline including 10 mM ethylenediamine tetraacetic acid disodium salt (pH 7.4) for 2 h at 4°C. They were then sliced (2 mm thickness) and fixed for an additional 4 h. The frozen specimens in

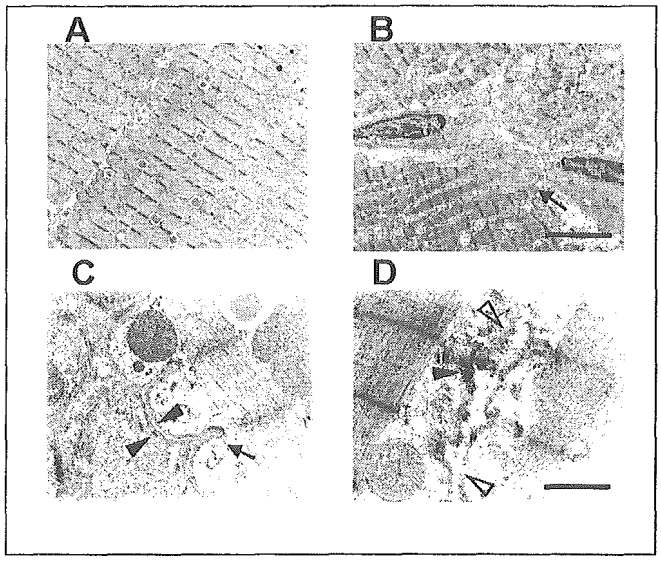

Figure 2) *Electron microscopy of a hamster heart of normal F1B (A,C) or hereditary DCM TO-2 strain (B,D) at the low-power magnification (original magnification ×5000; A,B) and the high-power magnification (original magnification ×25,000; C,D).* **A** *In the F1B heart, myofibrils were tightly arranged in parallel, mitochondria were homogeneous in size and located between myofibrils, and fibrotic change was minimal.* **B** *In a TO-2 strain sample, the myofibrils were disarranged, numerous bizarrely formed mitochondria were observed and the mitochondrial size was variable (closed arrows).* **C** *In the F1B heart, the sarcolemma was sharply demarcated (closed arrowheads) and the electron density of costameres was increased (closed arrows). The structure of myofilaments and cristae was well preserved.* **D** *In a TO-2 strain sample, the sarcolemma was widened and locally thickened (closed arrowheads) or disrupted without preserving the structure of the lipid bilayer (open arrowheads). Note that the increment of electron density was lost at costameres. Bar length indicates 0.2 μm (A,B) or 1 μm (C,D)*

OCT compound were prepared for the immunohistological assessment, as described previously (9,10). The samples were incubated overnight with primary monoclonal antibodies to dystrophin or with polyclonal antibodies to δ-SG at 4°C. After washing with Tris-buffered saline and incubating for 20 min at 37°C with the second antibody, the section was incubated with diaminobenzidine for 10 min at room temperature. Ultra-thin sections (60 nm thick) mounted on a copper grid and counterstained with uranyl acetate were examined with EM, as described earlier.

Antibodies

Site-directed polyclonal antibodies to δ-SG, of which an epitope was selected from a unique amino acid sequence deduced from the cloned cDNA, were raised in rabbits and purified by affinity chromatography, as described previously (2). Monoclonal antibodies to the rod domain of dystrophin were from Novocastra (Newcastle, United Kingdom). The second antibodies to the monoclonal and polyclonal primary antibodies from the mouse and rabbit, respectively, were labelled with horseradish peroxidase.

RESULTS AND DISCUSSION

EM

The ultrastructure of normal F1B hamster hearts at low-power magnification demonstrated tightly arranged cardiac muscle without noticeable fibrosis (Figure 2A). Mitochondria were homogeneous in size and neatly located between myofibrils or

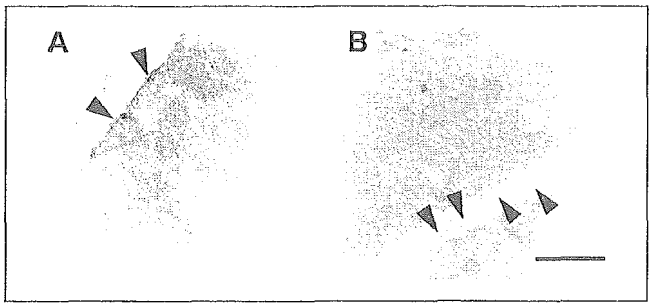

Figure 3) *Immuno-electron microscopy of* delta-sarcoglycan (δ-SG) *in F1B (A) and TO-2 (B) strain hearts at high-power magnification (original magnification ×25,000). Immunostaining of δ-SG revealed homogenous deposits along the sarcolemma in the normal heart (A, arrowheads), while it was not detected in the TO-2 heart (B, arrowheads). Bar length indicates 1 μm*

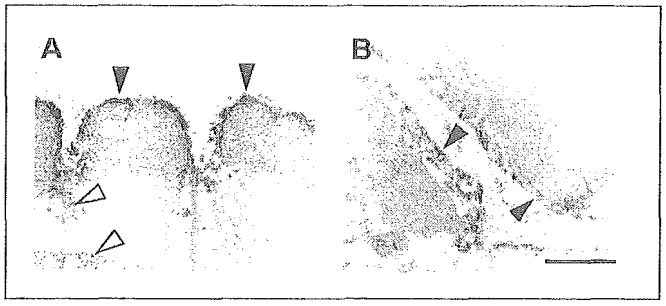

Figure 4) *Immuno-electron microscopy of dystrophin in F1B (A) and TO-2 (B) hamster hearts at high-power magnification (original magnification ×25,000).* **A** *In the normal heart, dystrophin revealed homogenous deposits along the sarcolemma (closed arrowheads) and the T-tubular system (open arrowheads).* **B** *In the TO-2 heart, immunodeposits of dystrophin were heterogeneously expressed (closed arrowheads). Bar length indicates 1 μm*

under the SL. In contrast, the TO-2 heart at the same age (25 weeks) was markedly dilated, and the myocardium showed interstitial fibrosis or calcification (12). Disarray and thinning of myofibrils were also noted (data not shown). The principle outcome of the EM studies was a multi-elemental pathology at subcellular levels. TO-2 samples showed that the myofibrils were unarranged, disrupted and degenerated. As described by Schaper et al (13) in human cases, the reduction of myofilaments was obvious. The interstitial space was widened and contained macrophages, fibroblasts, collagen fibres and cell debris in TO-2 hamsters. The I- and Z-bands showed disintegration. Bizarrely formed mitochondria were also observed and the size varied with the vacuolar degeneration and the proliferation. The cristae were loosely arranged or disrupted (Figure 2B). A wide variety of intra- and intercellular findings among myocardial cells were apparent (data not shown), similar to the results of previous reports (7,8).

We noticed the alteration of the SL at high magnification. EM of the control heart demonstrated sharply demarcated SL and tightly arranged myofibrils in parallel (Figure 2C). We identified two types of sarcolemmal degradation in TO-2 hearts (Figure 2D): widened and locally thickened SL, and a blurred and discontinuous lipid bilayer. The SL was poorly demarcated in some portions and discontinuous in other parts, where the basal lamina was not clearly observed. Myofibrils demonstrated frying of myofilaments with blurring of the I- and Z-band regions. As described by Jasmin and Eu (8), contraction bands adjacent to an intercalated disk were often encountered. Such severe involvement of peripheral fibrils is characterized by deep infoldings of the SL that enclose aberrant mitochondria to be eventually phagocytosed.

Immuno-EM

Immunostaining of δ-SG revealed homogenous deposits along the SL in F1B hearts (Figure 3A), whereas it was not detected in TO-2 hearts at all (Figure 3B). These results were in agreement with our report that the δ-SG gene showed a large deletion including the promoter region, exon 1 and intron 1 (2), and caused both genetic and morphological findings, as published previously (2,3,9,10). Figure 4A shows that immunostaining of dystrophin revealed deposits along the SL in the normal hamster, but the deposits were more densely detected just above Z-discs, at the costamere. We could not detect immunoproduct on Z-discs, as was reported by Kaprielian et al (14).

There has been both agreement and controversy over the precise location of dystrophin at the subcellular level. Many studies using immuno-EM or confocal microscopy confirmed that cardiac muscle shows dystrophin expression not only at the SL but also at the T-tubules (14-16); these findings were not observed in skeletal muscle, which demonstrates selective expression on the SL alone (17). However, the expression on Z-discs did not reach an agreement on the precise location of dystrophin. Present results in hamsters (Figure 4A) and recent reports in animals and humans reveal no expression on Z-discs (14,16). Meng et al (18) revealed the selective labelling of Z-discs with dystrophin antibodies. Because T-tubules are located close to Z-discs, more exact and careful evaluation is required.

As was distinctly demonstrated in Figure 4B, dystrophin appeared to be heterogeneously stained along the SL in TO-2 hearts. The immunoproduct showed patchy deposition along the fragile SL. The specific location of dystrophin to T-tubules and costameres was not evident in the present study. The amount of dystrophin appeared to be preserved at 15 weeks of age (9) but seemed to be decreased in the failing stage at 25 weeks of age. Accordingly, the age-dependent reduction rate of dystrophin was more gradual than SG complex (9).

In addition to dystrophin, other sarcolemmal proteins including L-type calcium channels (19,20), sodium-calcium exchangers (21) and sodium-potassium ATPases (22) have been reported to be reduced in failing hearts. These findings suggest that biosynthesis declined and/or the degradation rate of these proteins was accelerated under the pathological conditions. We need to be cautious of whether the decreases of these sarcolemmal proteins are directly related to the cause of the myocardial dysfunction or result from it.

The function of dystrophin may not be restricted to mechanical support for preventing overexpansion of the SL in repetitive systole to stabilize the SL (5). Considering the connection between dystrophin and neuronal nitric oxide synthase or caveolin (Figure 1), it is conceivable that dystrophin together with DRPs may serve signal transmission, such as myocardial hypertrophy secondary to cell stretching, volume overload or pressure loading. The latest report that the gene mutation of intranuclear protein, lamin A/C, also accompanies DCM, severe arrhythmias as well as mental retardation (23) would strongly suggest another aspect of DRP, because DRP is indirectly linked to lamin A/C via dystrophin and actin (24).

The leaky SL has already been reported in skeletal muscle in human patients with Duchenne-type muscular dystrophy and in mdx mice (25). Evans blue uptake, the marker of a leaky SL, was detected in cardiomyocytes in the cardiomyopathic hamster heart (10,26). We have already succeeded in the supplementation of a normal sequence δ-SG gene using long-lasting and harmless recombinant adeno-associated virus vector to the TO-2 strain hamster, and verified the restoration of both functional and morphological degeneration (9,10,12), amelioration of the permeability of the SL (10) and improvement in the animal's prognosis (10). These data provide evidence th the gene therapy is actually beneficial for fundamental tre ment of advanced heart failure, although more detailed ana sis is required to establish our scheme.

ACKNOWLEDGEMENTS: This study was financially suppc ed by grants-in-aid from the Ministry of Education, Scien Culture and Sports, the Ministry of Health, Labor and Welfa the Mitsubishi Research Foundation and the Motor Vehi Foundation.

REFERENCES

1. Homburger F, Baker JR, Nixon CW, Whitney R. Primary, generalized polymyopathy and cardiac necrosis in an inbred line of Syrian hamsters. Med Exp 1962;6:339-45.
2. Sakamoto A, Ono K, Abe M, et al. Both hypertrophic and dilated cardiomyopathies are caused by mutation of the same gene, δ-sarcoglycan, in hamster: An animal model of disrupted dystrophin-associated glycoprotein complex. Proc Natl Acad Sci USA 1997;94:13873-8.
3. Kawada T, Nakatsuru Y, Sakamoto A, et al. Strain- and age-dependent loss of sarcoglycan complex in cardiomyopathic hamster hearts and its re-expression by δ-sarcoglycan gene transfer in vivo. FEBS Letters 1999;458:405-8.
4. Tsubata S, Bowles KR, Vatta M, et al. Mutations in the human δ-sarcoglycan gene in familial and sporadic dilated cardiomyopathy. J Clin Invest 2000;106:655-62.
5. Cox GF, Kunkel LM. Dystrophies and heart disease. Curr Opin Cardiol 1997;12:329-43.
6. Bajusz E, Baker JR, Nixon CW, Homburger F. Spontaneous, heredity myocardial degeneration and congestive heart failure in a strain of Syrian hamster. Ann NY Acad Sci 1969;156:105-29.
7. Paterson RA, Layberry RA, Nadkarni BB. Cardiac failure in the hamster. A biochemical and electron microscopy study. Lab Invest 1972;26:755-66.
8. Jasmin G, Eu HY. Cardiomyopathy of hamster dystrophy. Ann NY Acad Sci 1979;317:46-58.
9. Kawada T, Sakamoto A, Nakazawa M, et al. Morphological and physiological restorations of hereditary form of dilated cardiomyopathy by somatic gene therapy. Biochem Biophys Res Commun 2001;284:431-5.
10. Kawada T, Nakazawa M, Nakauchi S, et al. Rescue of hereditary form of dilated cardiomyopathy by rAAV-mediated somatic gene therapy. Proc Natl Acad Sci USA 2002;99:901-6.
11. Kawaguchi H, Shin WS, Wang YP, et al. In vivo gene transfection of human endothelial cell nitric oxide synthase in cardiomyocytes causes apoptosis-like cell death. Circulation 1997;95:2441-7.
12. Toyo-oka T, Kawada T, Xi H, et al. Gene therapy prevents disruption of dystrophin related proteins in a model of hereditary dilated cardiomyopathies in hamster. Heart Lung Circ 2002;11:174-81.
13. Schaper J, Froede R, Hein S, et al. Impairment of the myocardial ultra structure and changes of the cytoskeleton in dilated cardiomyopathy. Circulation 1991;83:504-14.
14. Kaprielian RR, Stevenson S, Rothery SM, Cullen MJ, Severs NJ. Distinct patterns of dystrophin organization in myocyte sarcolemma and transverse tubules of normal and diseased human myocardium. Circulation 2000;101:2586-94.
15. Frank JS, Mottino G, Chen F, Peri V, Holland P, Tuana BS. Subcellular distribution of dystrophin in isolated adult and neonatal cardiac myocytes. Am J Physiol 1994;294:C1707-16.
16. Stevenson S, Rothery S, Cullen MJ, Severs NJ. Dystrophin is not a specific component of the cardiac costamere. Circ Res 1997;80:269-80.
17. Cullen MJ, Walsh J, Nicholson LVB, Harris JB. Ultrastructural localization of dystrophin in human muscle by using gold immunolabelling. Proc R Soc Lond 1990;240:197-210.
18. Meng H, Leddy JJ, Frank J, Holland P, Tuana BS. The association of cardiac dystrophin with myofibrils/Z-disc regions in cardiac muscle suggests a novel role in the contractile apparatus. J Biol Chem 1996;271:12364-71.
19. He J, Conklin MW, Foell JD, et al. Reduction in density of transverse tubules and L-type Ca2+ channels in canine tachycardia-induced heart failure. Cardiovasc Res 2001;49:298-307.
20. Chen X, Piacentino V 3rd, Furukawa S, Goldman B, Marguiles KB, Hauser SR. L-type Ca^{2+} channel density and regulation are altered in failing human ventricular myocytes and recover after support with mechanical assist devices. Circ Res 2002;91:517-24.
21. Sipido KR, Volders PG, Vos MA, Verdonck F. Altered Na/Ca exchange activity in cardiac hypertrophy and heart failure: A new target for therapy? Cardiovasc Res 2002;53:782-805.
22. Schwinger RH, Wang J, Frank K, et al. Reduced sodium pump α1, α3, and β1-isoform protein levels and N^+-K^+-ATPase activity but unchanged Na^+-Ca^{2+} exchanger protein levels in human heart failure. Circulation 1999;99:2105-12.
23. Fatkin D, MacRae C, Sasaki T, et al. Missense mutations in the rod domain of the lamin A/C gene as causes of dilated cardiomyopathy and conduction-system disease. N Engl J Med 1999;341:1759-62.
24. Towbin JA, Bowles NE. Sarcoglycan, the heart, and skeletal muscles: New treatment, old drug? J Clin Invest 2001;107:153-4.
25. Fong PY, Turner PR, Denetclaw WF, Steinhardt RA. Increased activity of calcium leak channels in myotubes of Duchenne human and mdx mouse origin. Science 1990;250:673-6.
26. Badorff C, Lee G-H, Lamphear BJ, et al. Enteroviral protease-2A cleaves dystrophin: Evidence of cytoskeletal disruption in an acquired cardiomyopathy. Nature Med 1999;5:320-6.

Translocation and cleavage of myocardial dystrophin as a common pathway to advanced heart failure: A scheme for the progression of cardiac dysfunction

Teruhiko Toyo-Oka*†‡§, Tomie Kawada¶, Jumi Nakata*, Han Xie*, Masashi Urabe‖, Fujiko Masui*, Takashi Ebisawa*, Asaki Tezuka*, Kuniaki Iwasawa†‡, Toshiaki Nakajima†, Yoshio Uehara†, Hiroyuki Kumagai**, Sawa Kostin††, Jutta Schaper††, Mikio Nakazawa‡‡, and Keiya Ozawa‖

*Department of Pathophysiology and Internal Medicine, †Health Service Center, and ‡Department of Cardiovascular Medicine, University of Tokyo, Tokyo 113-0033, Japan; ¶Division of Pharmacy and ‡‡Department of Medical Technology, Niigata University, Niigata 951-8520, Japan; ‖Division of Gene Therapy, Jichi Medical School, Tochigi 329-0498, Japan; **Department of Pharmacology, Gunma University, Maebashi 371-8511, Japan; and ††Department of Experimental Cardiology, Max Planck Institute, Bad Nauheim 61231, Germany

Communicated by Setsuro Ebashi, Okazaki National Research Institutes, Okazaki, Japan, March 25, 2004 (received for review January 24, 2004)

Advanced heart failure (HF) is the leading cause of death in developed countries. The mechanism underlying the progression of cardiac dysfunction needs to be clarified to establish approaches to prevention or treatment. Here, using TO-2 hamsters with hereditary dilated cardiomyopathy, we show age-dependent cleavage and translocation of myocardial dystrophin (Dys) from the sarcolemma (SL) to the myoplasm, increased SL permeability *in situ*, and a close relationship between the loss of Dys and hemodynamic indices. In addition, we observed a surprising correlation between the amount of Dys and the survival rate. Dys disruption is not an epiphenomenon but directly precedes progression to advanced HF, because long-lasting transfer of the missing *δ-SG* gene to degrading cardiomyocytes *in vivo* with biologically nontoxic recombinant adenoassociated virus (rAAV) vector ameliorated all of the pathological features and changed the disease prognosis. Furthermore, acute HF after isoproterenol toxicity and chronic HF after coronary ligation in rats both time-dependently cause Dys disruption in the degrading myocardium. Dys cleavage was also detected in human hearts from patients with dilated cardiomyopathy of unidentified etiology, supporting a scheme consisting of SL instability, Dys cleavage, and translocation of Dys from the SL to the myoplasm, irrespective of an acute or chronic disease course and a hereditary or acquired origin. Hereditary HF may be curable with gene therapy, once the responsible gene is identified and precisely corrected.

Despite the steady progress of pharmaceutical therapy, it is still difficult to completely prevent heart failure (HF) from proceeding to an advanced stage. Cardiac transplantation is the last choice to save the patient at the end stage, and this treatment entails many sociomedical problems. An alternative strategy for therapy is urgently required (1, 2). Primary or secondary degradation of dystrophin (Dys) might be of great significance in determining the cause of HF. Muscular dystrophy results in HF, and poor outcome in patients and animal models is associated with genetic mutations of Dys or the sarcoglycan (SG) complex (1–6). In the present study, we examined the following phenomena: (*i*) the time course of the hemodynamics with biventricular catheterization under stable anesthesia (7) until the TO-2 animals started to show overt HF and cardiac death; (*ii*) *in situ* sarcolemma (SL) stability by double fluoromicroscopy for the entry of an SL-impermeable dye, Evans blue dye (EB), into cardiomyocytes (8) and immunostaining of Dys or δ-SG; (*iii*) Western blotting of Dys and protein quantification; (*iv*) the correlation between limited proteolysis of Dys and hemodynamics; and (*v*) *in vivo* gene transduction in TO-2 hamsters. We also evaluated pathological features in rats with acute and acquired HF due to isoproterenol (Isp) toxicity (9) and in humans with advanced dilated cardiomyopathy (DCM).

Materials and Methods

Experimental Animals, the *rAAV* Vector Gene Construct, and *in Vivo* Gene Delivery. Male F_1B (control) and TO-2 hamster strains were obtained from Bio Breeders (Watertown, MA), and rAAV/lacZ vector alone or a mixture of recombinant adenoassociated virus (rAAV)/lacZ and rAAV/δ-SG was intramurally injected into the cardiac apex of the 5-week-old hamsters (7). pW1, an rAAV plasmid containing lacZ or a 1.2-kb fragment of δ-SG cDNA flanked by inverted terminal repeats of the AAV genome, pHLP19, a helper plasmid with *rep* and *cap* genes, and pladeno-1, a plasmid harboring the adenovirus *E2A*, *E4*, and *VA* genes, were used for rAAV/lacZ or rAAV/δ-SG production. pWSG with a δ-SG expression cassette driven by a cytomegalovirus (CMV) promoter was used for rAAV/δ-SG production (7, 8). Under open chest surgery with constant-volume ventilation, rAAV/lacZ alone or a mixture of rAAV/lacZ and rAAV/δ-SG was intramurally injected into the cardiac apex twice (each injection was 15 μl, for a total of 8.4×10^{10} and 6×10^{10} copies for lacZ and δ-SG, respectively).

Morphological and Immunological Analyses. A polyclonal, site-directed antibody to δ-SG was prepared at a high titer, by using a synthetic peptide with a sequence deduced from the cloned cDNA as a specific epitope (4). Monoclonal antibodies to Dys and to the transgene of lacZ (β-galactosidase) were obtained from NovoCastra (Newcastle, U.K.) and Funakoshi (Tokyo). The density of antibody-specific bands for the rod domain of Dys was measured within a linear intensity range for the applied amount of protein, after Western blotting of whole-heart homogenates, by 5–15% SDS/PAGE. For the Isp study, 10–20% SDS/PAGE was used to detect degradation products of both Dys and δ-SG. To simultaneously monitor Dys disruption, SL fragility *in situ*, and expression of the δ-SG transgene, double fluoromicroscopy was used to detect immunostaining of Dys with a FITC-labeled antibody specific to the rod domain of Dys, the entry of membrane-impermeable EB into cardiomyocytes, and immunostaining of δ-SG with a rhodium isothiocyanate (RITC)-labeled specific antibody by using a Nikon Diaphot or a Leica (Heidelberg, Germany) TCS SL confocal microscope. Where indicated, the Dys immunoproduct in the SL and myoplasm was semiquantified on cardiomyocytes, with or without transduction of δ-SG in the same observation field.

Abbreviations: HF, heart failure; Dys, dystrophin; SG, sarcoglycan; SL, sarcolemma; EB, Evans blue dye; Isp, isoproterenol; DCM, dilated cardiomyopathy; rAAV, recombinant adenoassociated virus; LVP, left ventricular pressure; EDP, end diastolic pressure; CVP, central venous pressure.

§To whom correspondence should be addressed. E-mail: toyooka_3im@hotmail.com.

Table 1. Cardiac hemodynamics with progression of HF

Strain	Age, weeks	LVP, mmHg	dP/dt_{max}, mmHg/sec	dP/dt_{min}, mmHg/sec	EDP, mmHg	CVP, mmHg
F_1B	5	82.9 ± 1.2	4,385 ± 91	−4,503 ± 208	3.1 ± 0.6	1.70 ± 0.53
	15	132.9 ± 5.5†	8,188 ± 743†	−7,188 ± 971†	1.8 ± 1.5	0.78 ± 0.50
	25	132.5 ± 6.9	6,709 ± 188	−6,513 ± 602	1.7 ± 2.7	0.46 ± 0.21
	40	125.1 ± 9.6	7,063 ± 290	−7,180 ± 576	1.6 ± 0.9	−0.62 ± 0.32
TO-2	5	83.0 ± 2.1	4,599 ± 192	−5,175 ± 233*	1.9 ± 0.3*	2.82 ± 0.17*
	15	100.2 ± 4.7*†	4,645 ± 637*	−3,664 ± 378*†	8.8 ± 1.9*†	2.70 ± 0.87*
	25	87.9 ± 8.3*	5,240 ± 388*	−3,171 ± 80*	12.8 ± 1.6*	3.12 ± 0.88*
	40	80.0 ± 2.8*	4,283 ± 97*	−3,120 ± 145*	18.0 ± 1.4*†	9.35 ± 1.35*†

Hemodynamic indices measured under stable anesthesia (7, 8): LVP, its maximum derivative (dP/dt_{max}) and minimum derivative (dP/dt_{min}), EDP, and CVP, in control (F_1B strain) and hereditary DCM (TO-2 strain) hamsters. Each value is shown as the mean ± SE (n = 4–8 hamsters in each group). * and † indicate statistical significance ($P < 0.05$) compared with the F_1B strain and the preceding age, respectively.

Hemodynamic Studies and Statistical Analyses. Peak left ventricular pressure (LVP), left ventricular end diastolic pressure (EDP), its first derivative (dP/dt), and central venous pressure (CVP) were measured under stable anesthesia (7, 8). All values were expressed as the mean ± SE and evaluated by paired Student's t test, ANOVA, and correlation analyses. A P value of <0.05 was considered significant.

Results and Discussion

Progression of DCM to Advanced HF in TO-2 Hamsters. Control F_1B hamsters showed growth-dependent increases in the peak LVP, the maximum rate of LVP (dP/dt_{max}), and the minimum rate of LVP (dP/dt_{min}, Table 1). In contrast, TO-2 hamsters persistently demonstrated systolic failure characterized by reduced LVP, dP/dt_{max}, and blunted dP/dt_{min}. Congestive HF was documented by increased left ventricular EDP and CVP. These signs became aggravated between 25 and 40 weeks of age, when the rate of cardiac death sharply increased (see below). The EDP and CVP reached levels 9.5 and 3.3 times higher, respectively, than those at 5 weeks of age.

Translocation of Dys from the SL to the Myoplasm During DCM Progression. Cardiac samples from TO-2 hamsters revealed time-dependent pathological features at each age (Fig. 1). After 5 weeks, double fluoromicroscopy showed that Dys was neatly arranged on the SL, and EB administered *i.v.* before killing the animals did not enter the myoplasm, indicating that the integrity of the SL was well preserved. After 25 and 40 weeks, the Dys on the SL became blurred, and some cardiomyocytes demonstrated a shift of Dys from the SL to the myoplasm. We refer to this phenomenon as "translocation" of Dys. These cardiomyocytes matched exactly with cells that took up EB (within ovals), denoting that the SL of the translocated cells leaked the exogenously applied dye.

Cleavage of Dys in Hamster Heart and in the Hearts of Humans with DCM. Western blotting of the myocardial homogenate with an antibody specific to the rod domain of Dys showed characteristic features (Fig. 2*a Left*). Normal hearts at 5 weeks of age showed a band at 430 kDa corresponding to normal Dys, and the staining intensity was preserved up to 40 weeks of age. Striking differences were observed in TO-2 hamsters, although at 5 and 15 weeks of age the staining pattern did not differ from that of the F_1B heart. However, at 25 weeks of age, extra bands were detected between 60 and 200 kDa (Fig. 2*a Left*), and the intensity of the Dys 430-kDa band started to decline. The intensity of this band was markedly reduced between 25 and 40 weeks of age, whereas the intensity of the 60-kDa band increased, mirroring the Dys band (Fig. 2*b*). The period of significant Dys cleavage matched exactly the periods when Dys translocation became

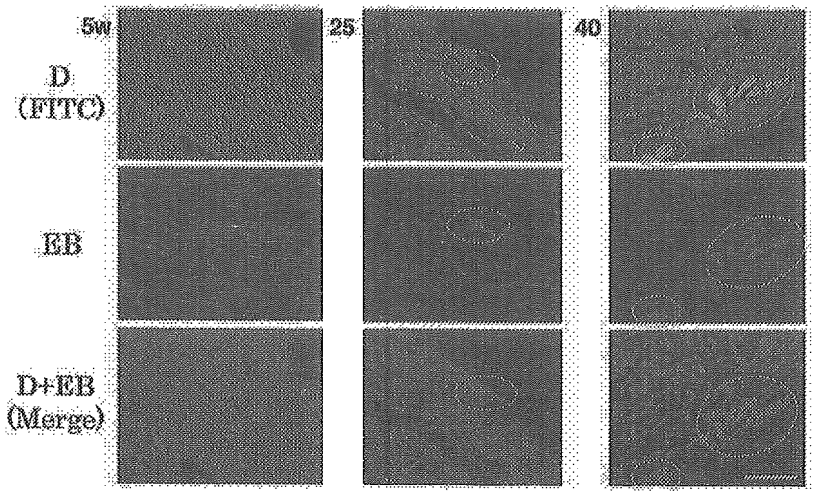

Fig. 1. Age-dependent translocation of Dys and increased permeability of the SL during HF progression in TO-2 hamsters. Double fluoromicroscopy for detection of a FITC-labeled antibody to the rod domain of Dys and entry of membrane-impermeable, fluorescent EB, at 5, 25, and 40 weeks of age (w). Cardiomyocytes demonstrating a shift of Dys from the SL to the myoplasm are shown in ovals. (Bar = 40 μm.)

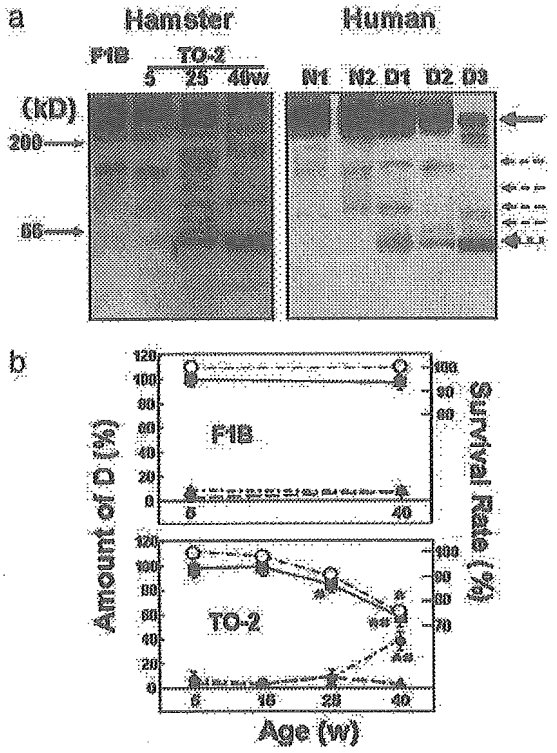

Fig. 2. Cleavage and reduction of cardiac Dys during DCM progression in hamsters and humans. (*a Left*) Control (F_1B strain) or DCM (TO-2 strain) hamsters at 5, 25, and 40 weeks of age (w). (*a Right*) Normal human myocardium (N1 and N2) and DCM hearts (D1, D2, and D3) at the time of cardiac transplantation. A solid arrow at 430 kDa and several dotted arrows denote the original Dys and its degradation products, respectively, after 5–20% SDS/PAGE of whole-heart homogenates. (*b*) Time course of the survival rate of control (F_1B; *Upper*) or DCM (TO-2; *Lower*) hamsters (○) and the density of immunoreactive bands specific to the rod domain of Dys at 430 (▩), 60 (●) or 160 (▲) kDa. * and # indicate a significant difference, compared with the control F_1B strain and the preceding age, respectively.

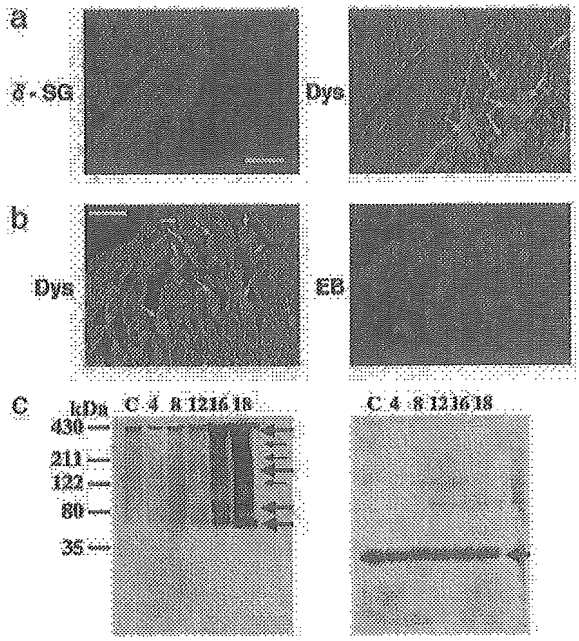

Fig. 3. (*a*) Double immunostaining of δ-SG (rhodamine isothiocyanate) and Dys (FITC) of TO-2 hamster hearts 35 weeks after local δ-SG gene transfection *in vivo* (8). Arrows indicate cardiomyocytes where dystrophin was translocated from the SL to the myoplasm. (Bar = 40 μm.) (*b*) Assessment of Dys translocation (FITC) and SL fragility *in situ* (EB entry) 16 h after the administration of Isp at a high dose (10 mg/kg i.p.) in Wistar rats (15). Arrows indicate cardiomyocytes where dystrophin was translocated from the SL to the myoplasm. (Bar = 40 μm.) (*c*) Western blotting of Dys (*Left*) and δ-SG (*Right*) from the same rat heart homogenate sample after gradient 10–15% SDS/PAGE of the control (C) and 4, 8, 12, 16 and 18 h after Isp treatment. Arrows indicate uncleaved Dys (430 kDa) and Dys degradation products (*Left*) or δ-SG (*Right*).

evident (Fig. 1) and when the animals started to die of congestive HF (ref. 8 and Fig. 2*b*). The intensity of the faint 160-kDa band did not change throughout the study and appeared to be unrelated to the progression of HF.

Similar cleavage of Dys was confirmed in hearts from patients with DCM of unidentified etiology who had undergone cardiac transplantation (Fig. 2*a Right*). The topological shift of Dys was also documented in samples of advanced stage DCM (unpublished data). Accordingly, the translocation was common to both animal models and patients with DCM. Other antibodies to the C or N terminus of Dys did not clearly recognize the cleavage product (data not shown). At present, we do not know the reason for this discrepancy in human cases of advanced HF showing selective cleavage of Dys at the N terminus (10).

Relationship of Dys Cleavage to Hemodynamics and the Lifespan of Hamsters. Surprisingly, the amount of Dys or its 60-kDa-band degradation product in TO-2 animals very closely correlated with the hemodynamic indices that characterize the progression of HF. The Dys amount was positively correlated with the systolic index [peak LVP, coefficient of regression (r) = 0.998 and $P < 0.0004$], and negatively correlated with the diastolic parameters (EDP, $r = 0.996$ and $P < 0.0005$; CVP, $r = 0.954$ and $P < 0.002$). The intensity of the 60-kDa band showed a clear negative correlation with the LVP ($r = 0.961$, $P < 0.002$) and a positive correlation with the EDP ($r = 0.954$, $P < 0.002$) and CVP ($r = 0.996$, $P < 0.0005$). These highly significant regression coefficients for correlation of the amount of Dys with systolic or diastolic performance support a tentative role for Dys in transmitting an effect through the actin–myosin linkage to the extracellular matrix. It is also noteworthy that no correlation was found between the amounts of Dys or the 60-kDa band and the dP/dt_{max} or dP/dt_{min} value (data not shown), both of which are regulated by Ca^{2+} handling (11) and the energetics of cardiac muscle cells (12). It should be emphasized that a distinct relationship was found between the amount of Dys or the 60-kDa band and the survival rate of the TO-2 animals over time (Fig. 2*b Lower*). It is possible that these immunological and hemodynamic data could be biased, because ≈30% of the TO-2 hamsters died of HF (Fig. 2*b Lower*), and we could only use the survivors in the analysis.

Effect of Long-Lasting Gene Therapy on Dys Localization. The final evidence that the disruption of Dys is not an epiphenomenon in HF but is actually caused by a loss of δ-SG is provided by the double immunostaining of Dys and δ-SG in TO-2 hearts with or without local gene transfection *in vivo* (Fig. 3*a*). In control F_1B hearts, both proteins were equally expressed on the SL (data not shown). In contrast, the TO-2 heart did not express δ-SG (13). As described above (Fig. 1), Dys staining became blurred with age, and some cardiomyocytes revealed Dys translocation (14). Gene delivery of normal δ-SG *in vivo*, by means of a nonpathogenic and long-lasting rAAV vector (7, 8), was used to locally express the δ-SG transgene, and this gene therapy completely ameliorated Dys translocation in the same cardiomyocytes for up to 35 weeks (Fig. 3*a Left*). In contrast, nontransfected cells

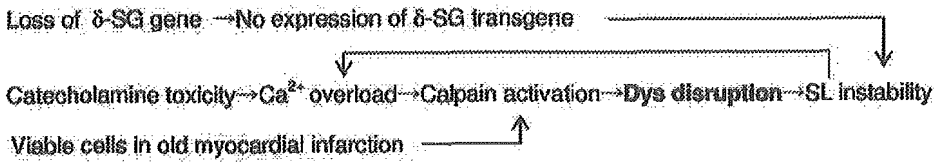

Scheme 1. Pathways for the progression of HF to an advanced stage.

showed translocation of Dys in the same sample (indicated by arrows in Fig. 3*a Right*). This finding specifically eliminates the possibility that Dys disruption resulted from the parallel development of HF, because Dys translocation was restricted to cardiomyocytes that did not express the δ-SG transgene. Furthermore, the amount of Dys estimated *in situ* by densitometry of immunofluoromicroscopic images in cardiomyocytes indicated a 1.22 ± 0.13 fold ($P < 0.01$) preferential localization of Dys on the SL of δ-SG-transfected cells ($n = 70$ cells per group).

Effect of Isp on SL Permeability, and Shift and Cleavage of Dys and δ-SG. A toxic dose of Isp (10 mg/kg i.p.) causes acute HF and morphological deterioration in normal rats (9). Pathological examination has shown time-dependent degradation of Dys and apoptosis of cardiomyocytes from 4 to 18 h after Isp was administered (15). Confocal microscopy of cardiomyocytes in the same observation field showed translocation of Dys (indicated by arrows in Fig. 3*b Left*) and entry of the SL-impermeable EB into the myoplasm of cardiac muscle cells. The shift of Dys was selectively detected 16 h after Isp treatment only in cardiomyocytes where EB had entered the myoplasm (Fig. 3*b Right*). Western blotting revealed time-dependent cleavage of Dys, showing degradation fragments between 60 and 200 kDa (Fig. 3*c Left*). In contrast, δ-SG was not hydrolyzed at all (Fig. 3*c Right*). Immunohistology confirmed that δ-SG did not shift from the SL but remained localized on the SL (data not shown). The effect of high-dose Isp, a β-adrenergic agonist, was similar to that observed in a DCM mouse with a protein kinase A knock-in gene (16). To verify the therapeutic effect of gene therapy in a β-adrenergic agonist/protein kinase A/phospholamban system, the pharmacological action (17, 18) and the disease prognosis need to be precisely examined, because an improvement in hemodynamics does not always prolong the lifespan of the animal (19).

The limited hydrolysis of Dys, common to the models of acute and chronic diseases in the present study, suggests a role for calpain, because cardiomyocytes contain an appreciable amount of this protein (20), and intracellular Ca^{2+} handling is modified in failing hearts (21, 22). Neither a specific inhibitor for calpain nor a calpain knockout animal is currently available to test this hypothesis. β-Adrenergic agonists induce Ca^{2+} overload in cardiomyocytes by increasing Ca^{2+} uptake (23). In addition, Dys and α-, β-, and γ-SG, but not δ-SG, are hydrolyzed by the endogenous protease (24) or isolated calpain *in vitro* (25, 26). The preferential breakdown of these proteins, but not δ-SG, in three HF models, i.e., TO-2 hamster hearts (13), Isp-treated rat hearts (Fig. 3*b*), and viable cells at the end stage of myocardial infarction (26), might be accompanied by substantially enhanced activity of *m*-calpain over its endogenous inhibitor, calpastatin. The expression of *m*-calpain in TO-2 hearts markedly exceeded that of calpastatin during the progression of HF (data not shown). These results may imply that the balance between calpain and calpastatin will shift in a calpain-dominant manner. Furthermore, dot hybridization analyses revealed no increment of mRNA of each DAP component under these HF conditions, suggesting that compensatory biosynthesis did not occur in the case of DAP.

A Scheme for the Progression of HF to an Advanced Stage. The clinical link between excess stimulation with catecholamines and myocardial damage has been confirmed by the therapeutic success of β-adrenergic antagonists in TO-2 hamsters (27) and humans (28, 29). The cleavage of Dys has also been documented after enterovirus infection, resulting in DCM-like HF (30). These pathological findings present a paradigm in which cardioselective cleavage of Dys may lead to progression of HF to an advanced stage (Scheme 1). Scheme 1 does not exclude the involvement of a protease cascade, as seen through the activation of a calpain-like homologue in neuronal degeneration in *Caenorhabditis elegans* (31), or involvement of the ubiquitin/proteasome system (32) in the loss of Dys. More definite evidence is required to precisely determine the causative factor(s). This common pathological process, irrespective of the hereditary or acquired origin and the chronic or acute course of the disease, suggests a strategy for the treatment of advanced HF through interruption of the vicious circle by either gene therapy or drug treatment.

We thank Dr. John R. Solaro (Department of Physiology and Biophysics, University of Illinois, Chicago) for discussion of the results and Dr. Y. Niwa and K. Kurosawa (Department of Pathophysiology, University of Tokyo) for experimental and secretarial assistance. This work was supported by Ministry of Education, Culture, and Science Grant A2 142070333 and by the Ministry of Welfare and Labor, Japan, the Mitsubishi Research Foundation, and the Motor Vehicle Foundation.

1. Cox, G. F. & Kunkel, L. M. (1997) *Curr. Opin. Cardiol.* **12**, 329–343.
2. Seidman, J. G. & Seidman, C. (2001) *Cell* **104**, 557–567.
3. Durbeej, M. & Campbell, K. P. (2002) *Curr. Opin. Genet. Dev.* **12**, 349–361.
4. Sakamoto, A., Ono, K., Abe, M., Jasmin, G., Eki, T., Murakami, Y., Masaki, T., Toyo-oka, T. & Hanaoka, F. (1997) *Proc. Natl. Acad. Sci. USA* **94**, 13873–13878.
5. Nigro, V., Okazaki, Y., Belsito, A., Piluso, G., Matsuda, Y., Politano, L., Nigro, G., Ventura, C., Abbondanza, C., Molinari, A. M., *et al.* (1997) *Hum. Mol. Genet.* **6**, 601–607.
6. Tsubata, S., Bowles, K. R., Vatta, M., Zintz, C., Titus, J., Muhonen, L., Bowles, N. E. & Towbin, J. A. (2000) *J. Clin. Invest.* **106**, 655–662.
7. Kawada, T., Sakamoto, A., Nakazawa, M., Urabe, M., Masuda, F., Hemmi, C., Wang, Y., Shin, W. S., Nakatsuru, Y., Sato, H., *et al.* (2001) *Biochem. Biophys. Res. Commun.* **284**, 431–435.
8. Kawada, T., Nakazawa, M., Nakauchi, S., Yamazaki, K., Shimamoto, R., Urabe, M., Nakata, J., Masui, F., Nakajima, T., Suzuki, J., *et al.* (2002) *Proc. Natl. Acad. Sci. USA* **99**, 901–906.
9. Kahn, D. S., Rona, G. & Chappel, C. I. (1969) *Ann. N.Y. Acad. Sci.* **156**, 285–293.
10. Vatta, M., Stetson, S. J., Perez-Verdia, A., Entman, M. L., Noon, G. P., Torre-Amione, G., Bowles, N. E. & Towbin, J. A. (2002) *Lancet* **359**, 936–941.
11. Ebashi, S., Nonomura, Y., Toyo-oka, T. & Katayama, E. (1976) *Symp. Soc. Exp. Biol.* **30**, 349–360.
12. Toyo-oka, T., Nagayama, K., Suzuki, J. & Sugimoto, T. (1992) *Circulation* **86**, 295–301.
13. Kawada, T., Nakatsuru, Y., Sakamoto, A., Koizumi, T., Shin, W. S., Okai-Matsuo, Y., Suzuki, J., Uehara, Y., Nakazawa, M., Satoh, H., *et al.* (1999) *FEBS Lett.* **458**, 405–408.
14. Kawada, T., Hemmi, C., Fukuda, S., Iwasawa, K., Tezuka, A., Nakazawa, M., Sato, H. & Toyo-oka, T. (2004) *Exp. Clin. Cardiol.* **8**, in press.
15. Xi, H., Shin, W. S., Suzuki, J., Nakajima, T., Kawada, T., Uehara, Y., Nakazawa, M. & Toyo-oka, T. (2000) *J. Cardiovasc. Pharmacol.* **36**, Suppl. 2, S25–S29.
16. Antos, C. L., Frey, N., Marx, S. O., Reiken, S., Gaburjakova, M., Richardson, J. A., Marks, A. R. & Olson, E. N. (2001) *Circ. Res.* **89**, 997–1004.